UNIVERSIDAD AUTÓNOMA DE NUEVO LEÓN

FACULTAD DE CIENCIAS QUÍMICAS

Fluorescent sensing of Cr (III) using benzotriazolyl vinyl anilines

Por:

LQI. GREGORIO HUMBERTO VILLARREAL QUIROGA

Como requisito para obtener el grado de Maestría en Ciencias con orientación en Química de los Materiales

Monterrey, Nuevo León, Agosto, 2024

Fluorescent sensing of Cr (III) using benzotriazolyl vinyl anilines

Aprobación de la tesis:

DR. ISRAEL ALEJANDRO LÓPEZ HERNÁNDEZ
Presidente

DRA. THELMA ELIZABETH SERRANO QUEZADA
Secretario

DR. ALEJANDRO VÁZQUEZ DIMAS
Vocal

DRA. MARÍA ELENA CANTÚ CÁRDENAS
Subdirectora de Posgrado

Fluorescent sensing of Cr (III) using benzotriazolyl vinyl anilines

Revisión de la tesis:

DR. EUGENIO HERNÁNDEZ FERNÁNDEZ
Codirector de tesis

DRA. THELMA ELIZABETH SERRANO QUEZADA
Comité Tutorial

DR. ALEJANDRO VÁZQUEZ DIMAS
Comité Tutorial

DR. CARLOS EDUARDO PUENTE DE LEÓN
Comité Tutorial

DRA. MARÍA ELENA CANTÚ CÁRDENAS
Sub-Directora de Posgrado

Acknowledgements

I would like to thank Universidad Autónoma de Nuevo León and Facultad de Ciencias Químicas for providing the facilities needed to finish this project. I also want to thank CONAHCYT for giving me a scholarship (CVU No. **123681**).

I kindly thank both of my advisors Dr. Israel López and Dr. Eugenio Hernández for their time and patience while guiding me with this project. Also, I want to thank my tutorial committee, Dra. Thelma Serrano, Dr. Alejandro Vázquez and Dr Carlos Puente for all their valuable input that helped improve this work. I express my gratitude to the research group, Organic Synthesis Group, specially to the friends I made while working in the laboratory. I also want to thank all the students that have worked with me, helping in this or other projects.

I would like to thank my family, friends and pets for all their support.

Resumen

Gregorio Humberto Villarreal Quiroga Fecha de Graduación: Agosto 2024
Universidad Autónoma de Nuevo León
Facultad de Ciencias Químicas
Título del Estudio: **Fluorescent sensing of Cr (III) using benzotriazolyl vinyl anilines**

Número de páginas: 56 Candidato para el grado de Maestría en Ciencias con Orientación en Química de los Materiales

Área de Estudio: Química de los Materiales

Propósito y Método de Estudio: La contaminación del medio ambiente por metales pesados ha sido un problema grave para el ambiente y la salud. El cromo es uno de los contaminantes más comunes en México. Por lo tanto, en este proyecto se sintetizaron nuevos materiales orgánicos capaces de determinar este metal en soluciones acuosas por medio de la espectroscopía de fluorescencia.

Contribuciones y conclusiones:
Los sensores fueron sintetizados con éxito por medio de síntesis asistidas por microondas. Los compuestos presentaron cambios en sus propiedades fotofísicas con Cr (III), lo que los vuelve candidatos como sensores. Las pruebas de posibles interferencias mostraron que **BTZ-COOH** no presenta interferentes, mientras que Cu (II) es un interferente para el sensado con **BTZ-O**. La estequiometría entre Cr (III) y los compuestos fueron 2:3 y 1:1 para **BTZ-COOH** y **BTZ-O**, respectivamente. No existió correlación lineal entre la concentración de Cr (III) en presencia de los compuestos y la intensidad de fluorescencia para ambos compuestos.

Dr. Israel Alejandro López Hernández
Director de tesis

Dr. Eugenio Hernández Fernández
Codirector de tesis

Summary

Gregorio Humberto Villarreal Quiroga Graduation Date: August 2024
Universidad Autónoma de Nuevo León
Facultad de Ciencias Químicas
Study's Title: **Fluorescent sensing of Cr (III) using benzotriazolyl vinyl anilines**

Number of Pages: 56

Candidate for MSc. Chemistry of Materials degree

Study's Field: Material's Chemistry

Purpose and Study Methods: Pollution by heavy metals represents a public health and environmental risk. Chromium is one of the most common pollutants in México. Hence, two new materials capable of sensing metal ions in solution were synthesized in this project. These materials are capable of sensing metal ions by fluorescence spectroscopy.

Contributions and Conclusions:
The probes were successfully synthesized by means of microwave-assisted synthesis. The compounds exhibited changes in their photophysical properties with Cr (III), making them candidates as sensors. Interference tests showed that **BTZ-COOH** did not have interferents, while Cu (II) is an interferent for **BTZ-O**. Stoichiometry between Cr (III) and the compounds was determined to be 2:3 and 1:1 for BTZ-COOH and BTZ-O respectively. The concentration of Cr (III) in presence of the compounds and the fluorescence intensity did not show a linear correlation.

Dr. Israel Alejandro López Hernández
Advisor

Dr. Eugenio Hernández Fernández
Co-advisor

Fluorescent sensing of Cr (III) using benzotriazolyl vinyl anilines

Presented by:

LQI. Gregorio Humberto Villarreal Quiroga

The present research project was done at Laboratorio de Química Industrial, of Centro de Laboratorios Especializados (CELAES) of Facultad de Ciencias Químicas, UANL, under the supervision of Dr. Israel Alejandro López Hernández and Dr. Eugenio Hernández Fernández, with resources given by Consejo Nacional de Humanidades, Ciencias y Tecnologías (CONAHCYT) with the project CF-2023-I-1693 and scholarship 829156.

Table of contents

List of Schemes

List of Figures

List of Tables

1 Introduction

Environmental pollution has existed since before the beginning of the industrial revolution (1), but thanks to the technological and industrial advances this issue has grown dramatically. This long-lasting problem represents a global public health crisis, causing about 9 million deaths each year (2). In this context, Mexico has experienced a huge growth in population and great development of the industrial sector. This progress has caused more than 60% of the river systems in this country to show signs of pollution by heavy metals, pesticides, fertilizers, and wastewater effluents (3).

Out of the mentioned pollutants, heavy metal pollution has had a focus in attention due to their high toxicity, non-biodegradable nature, and high persistency. Arsenic, cadmium, chromium, lead, and mercury are the most important contaminants in Mexico in this category due to their natural high abundance (4). Proving the importance of new materials that can determine the presence and concentration of heavy metals in the environment.

1.1 Chromium

Chromium (Cr) is a naturally occurring element, found mostly in its trivalent and hexavalent forms. Found mainly in three minerals: chromite, crocoite and lopezite, this element is used in various industrial settings (5). In the metallurgical industry, this metal is used in the production of stainless steel, special purpose alloys, and metal plating, since this metal helps increase the hardness, overall strength, and corrosion resistance of these materials. On the other hand, this metal has also been used as an inorganic pigment in paint, varnishes, and oil colors (6).

1.1.1 Effects of chromium in health and environment

Chromium (III) is considered a micronutrient and plays a key role in metabolic processes, such as the breakdown of fats and carbohydrates, fatty acid and cholesterol synthesis and insulin action. In high concentrations, this oxidation

state has moderate toxicity. Chronic exposure causes perforation and ulcers in the respiratory system (7).

On the other hand, chromium (VI) is extremely toxic for humans, for both acute and chronic exposure. In this valence state it acts as a powerful oxidant, thus irritating the exposure route. Chronic exposure affects the lungs, kidney, liver, and other organs with the potential of causing cancer (8).

Chromium speciation in the environment has been extensively studied. Cr (III) is the most stable form found in nature, but due to its insolubility it is found mostly in soil and sediments. Chromium (VI) on the other hand is soluble in water, thus mobility in the environment takes place (9). Research has shown that depending on the chemical species found in nature, redox reactions of chromium can take place, oxidizing to chromate or reducing to chromium (III) (10).

1.1.2 Potential exposure routes

Due to its extensive use in industries, it was estimated in the year 2012 that 300,000 workers are annually exposed to chromium and its compounds (11). The main ways of exposure that have been documented are inhalation, ingestion, and skin contact (12).

On the other hand, this metal enters the environment through a variety of natural and anthropogenic sources, including mining, smelting, and metal processing. Among the sources of pollution, tanning is one of the most harmful to the environment. The tanning process of leather only uses 60-75% of the administered element, thus the discharged wastewater still contains this element and contaminates the environment (13).

Similarly, air quality reports have shown that airborne particulate matter (PM) may contain Cr, predominantly in its hexavalent form (14). This source of pollution is also very dangerous as fine particles can travel long distances and helps in the pollution of soil and water.

1.2 Methods of analysis

Due to its environmental and anthropogenic importance, many methods of quantification have been developed. As science and technology have advanced, these methods have evolved from classical volumetric and gravimetric analyses to the more complex instrumental methods. As can be seen in **Table 1**, both classical and instrumental methods have been used to determine the concentration of Cr. These methods although reliable, can have many disadvantages like errors in measurements due to interferences, high cost or high time consumption; that is why in recent years there have been studies focusing on quantifying metal ions with fluorescence spectroscopy (15).

Table 1. Comparison between methods for analyzing Cr.

	Volumetric	Gravimetric	Colorimetric	AAS	ICP-OES
Cr (III)	Back titration with complexation equilibrium,	Precipitation and ignition to obtain Cr_2O_3	Colored complex analysis.	Analyzes total Cr if no separation methods are used.	
Cr (VI)	Direct titration with redox equilibrium.	Precipitation of insoluble chromate salts with Hg, Pb, Ba, Ag.	Direct measurement at 350 nm.		
Detection	Visual color change	Weight of solid	Photodiode	Photomultiplier tube	
Advantages	Low cost and accessible	Low cost and accessible	Detection in ppm	Detection in ppm. Selectivity	
Disadvantages	Many interferences and errors due to indicator color change.	Coprecipitation can cause errors in measurement.	Absorption of other chemicals can cause errors.	High cost, time consuming, and specialized training is required.	
References	(16,17)	(18)	(19)	(20)	(21)

1.3 Fluorescent organic probes

1.3.1 Fluorescent spectroscopy

Fluorescence spectroscopy consists in the irradiation of a sample with monochromatic light and the subsequent detection of a spectrum of light. As explained in the Jablonski's diagram (**Figure 1**), when a molecule absorbs light, electrons are promoted from the ground state (S_0) to the excited states (S_n). After energy loss due to internal conversion and vibrational relaxation, electrons in the S_1 excited state return to the ground state after a radiative relaxation, producing a spectrum of fluorescence emission (22).

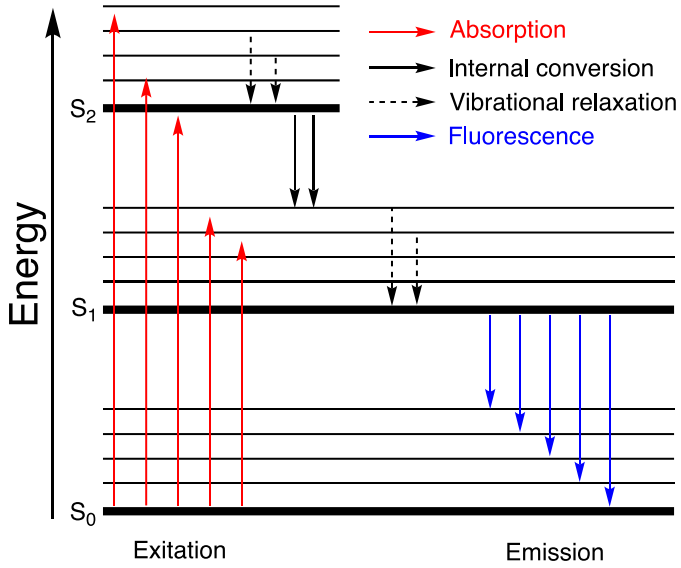

Figure 1. Jablonski diagram depicting the fluorescence process.

1.3.2 Push-pull system

An important aspect in the design of fluorescent organic molecules is the structural configuration and choice of motifs. One design, called the push-pull system (**Figure 2**), where a molecule contains an electron donating group (EDG) and an electron withdrawing group (EWG) connected by an unsaturated system. This structure ensures that after the light absorption takes place, the EDG transfers its electrons towards the EWG, thus creating a highly dipolar state (23).

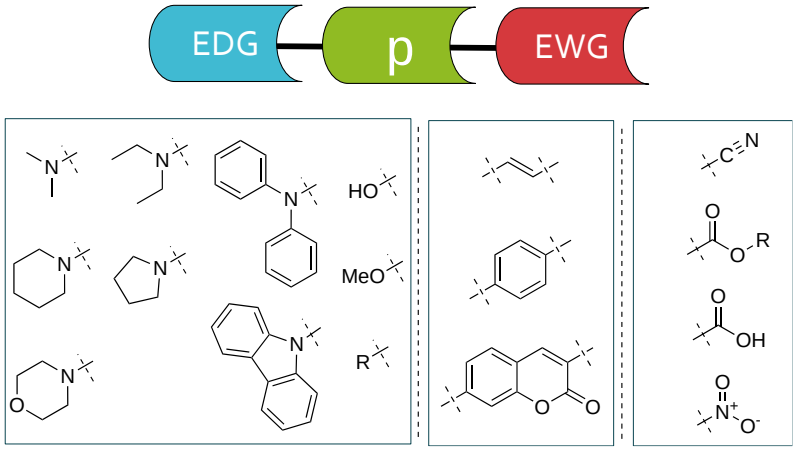

Figure 2. Examples of functional groups used in push-pull systems.

These and other types of fluorescent organic molecules have been used in organic light-emitting diodes (OLED) as the emissive layer (24,25), in bioimaging as organelle dyes (26), in dye-sensitized solar cells (DSSC) (27) and as chemical probes (28,29). Specifically, the use of organic molecules as sensors has brought many advantages to the analytical field. These compounds undergo a change in the photophysical properties (*e.g.* enhancement or quenching of fluorescence) due to interactions with specific chemical species. This specificity, the lack of background noise and the correlation of fluorescence intensity and concentration of analyte makes this spectroscopy a promising alternative for quantifying chemicals (30).

1.3.3 Sensors for metal ions

Organic molecules used as sensors for metal ions are commonly designed to promote coordination between the molecule and the metal ion. After coordination with a transition metal, the new metal complex will exhibit different photophysical properties due to relaxation of ligand-to-metal (LMCT) or metal-to-ligand (MLCT) excited states (30).

Reports in literature show that the most sought effects for these types of sensors are chelation enhanced fluorescence effect (CHEF) and chelation enhanced

quenching effect (CHEQ) which can be explained by various fluorescence mechanisms.

Some of the main mechanisms in which a sensor presents CHEF are:

- Photoinduced electron transfer (PET): Molecules are built to contain a fluorophore (in charge of producing fluorescence) and an ionophore (in charge of bonding to ions). In its free state, the compound is weakly or non-fluorescent due the PET effect. Upon excitation, electrons from the ionophore, that are of higher energy than the HOMO of the fluorophore, drop down to the HOMO of the fluorophore, inhibiting the free radiative relaxation of the fluorophore. When the molecule is bound to a metal ion, the electrons of the ionophore are stabilized to a lower energy than the fluorophore's HOMO, thus inhibiting the PET effect (**Figure 3**) (31).

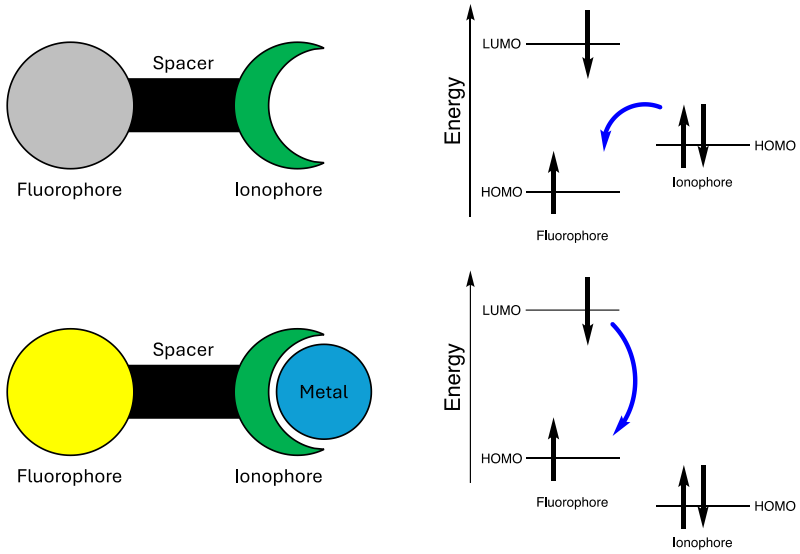

Figure 3. Depiction of the PET effect of fluorescent probes for metal ions.

- Excited state intramolecular proton transfer (ESIPT): These types of molecules have a proton donating and accepting group. The excited state of the enol-form of the molecule stabilizes quickly by transferring the proton, thus obtaining the keto-form and exhibiting fluorescence with large stokes shift. When the keto-form of the molecule relaxes, the enol-form is

spontaneously recovered by reverse proton transfer. When a metal coordinates, it removes the proton and the ESIPT effect is inhibited, and a significant blue shift of the fluorescence will be observed (**Figure 4**) (30).

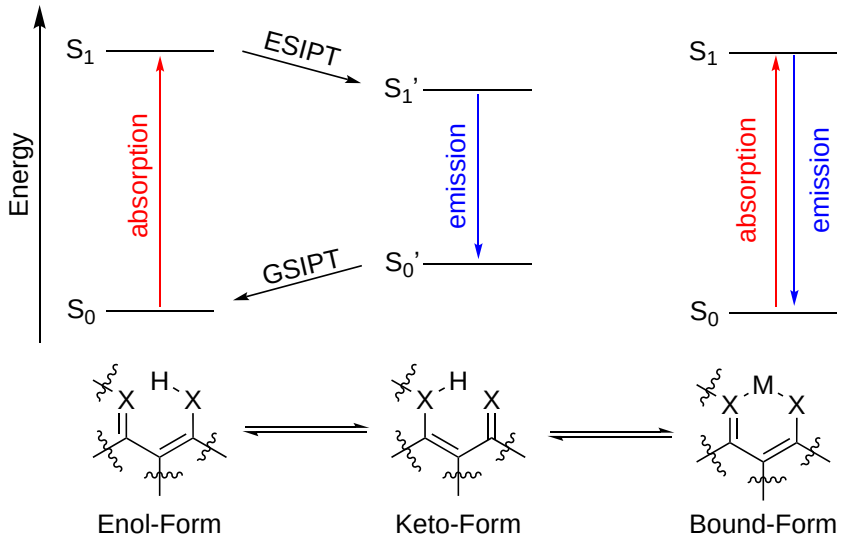

Figure 4. Depiction of the ESIPT effect of fluorescent probes for metal ions.

On the other hand, the CHEQ effect is usually explained by the paramagnetic fluorescence quenching mechanism. When a paramagnetic metal ion, like Cu^{2+} or Cr^{3+}, binds to a ligand, the partially filled d-orbitals of the metal center can be of higher energy than the HOMO orbital of the ligand. When the excited molecule relaxes, d-orbital electrons drop down to the HOMO orbital, thus inhibiting the fluorescence of the molecule (**Figure 5**) (32).

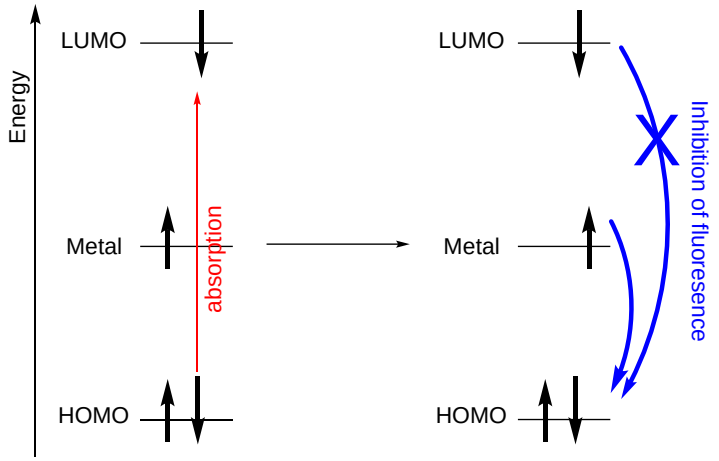

Figure 5. Depiction of paramagnetic fluorescence quenching effect.

In resume, heavy metal ions, such as Cr, are a worldwide environmental and public health risk, which arises the need to have better and less costly quantification techniques. Fluorescent probes have been studied as an alternative due to their low limits of detection, high selectivity, and low cost.

In this sense, two benzotriazolyl vinyl aniline derivatives (**Figure 6**) were synthesized and evaluated as sensors for Cr (III). The probes were designed to contain a push-pull system, where the EDG is dimethylamine, the EGW is either carboxylic acid or oxadiazole, and benzotriazole will help promote coordination with Cr (III) and the EWGs.

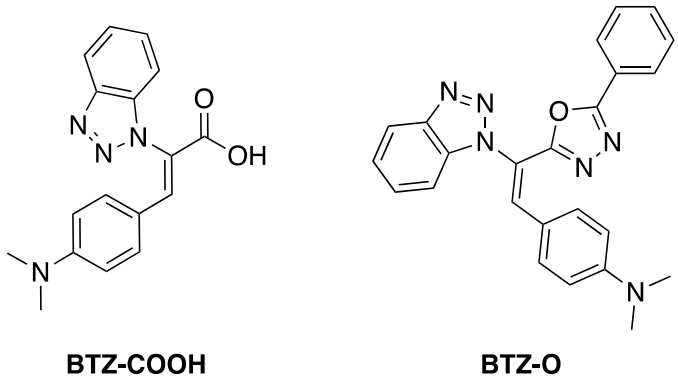

Figure 6. Benzotriazolyl vinyl aniline derivatives used as fluorescent Cr (III) sensors.

2 Background

2.1 Metal ion sensors

In recent years many reports of Cr (III) organic sensors have been published. These sensors have been built with different functional groups to selectively bind this metal ion.

In 2011, Karak D. *et al.* used 9-acridone-4-carboxilic acid as an efficient Cr (III) ion fluorescent sensor with negligible interferences (**Scheme 1**). This probe exhibited CHEQ effect upon binding with Cr (III) ion with a 2:1 stoichiometry. The linear range was found to be 1-9 μM using the compound at a concentration of 1 μM (33).

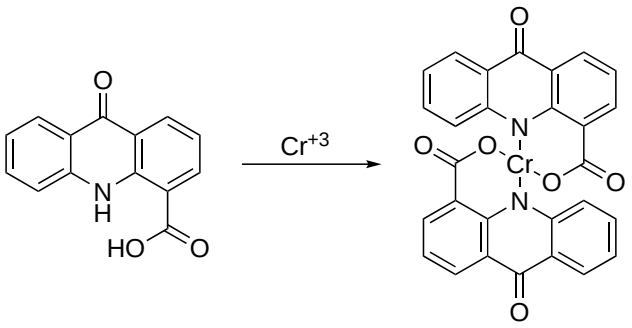

Fluorescent Non-fluorescent

Scheme 1. Binding mode of 9-acridone-4-carboxilic acid with Cr (III) ions.

In 2021, Seenan S. *et al.* synthesized a furan based fluorescent probe capable of sensing Cr (III) ions (**Scheme 2**). This sensor showed weak fluorescence at 405 nm and upon binding an increase in fluorescence by 5 times was observed. The stoichiometry was calculated by Job's plot to be 1:1. The limit of detection (LOD) for Cr (III) ions was found to be 0.142 μM (34).

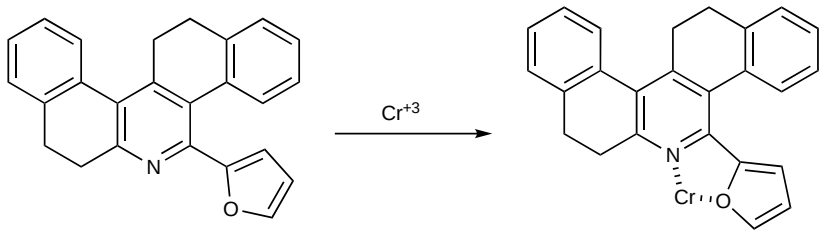

Non-fluorescent Fluorescent

Scheme 2. Binding mode of furan derivative with Cr (III) ions.

In 2020, Kolcu F. *et al.* synthesized a Schiff base, containing triphenyl and bithiophene units, as a fluorescent sensor for Cr (III) detection (**Scheme 3**). This probe presented a CHEF effect at 471 nm with a 59-fold increase at an excitation wavelength of 320 nm. The LOD value was 1.5 μM for Cr (III) ions with a 2:1 binding stoichiometry. No interferences were reported for this sensor (35).

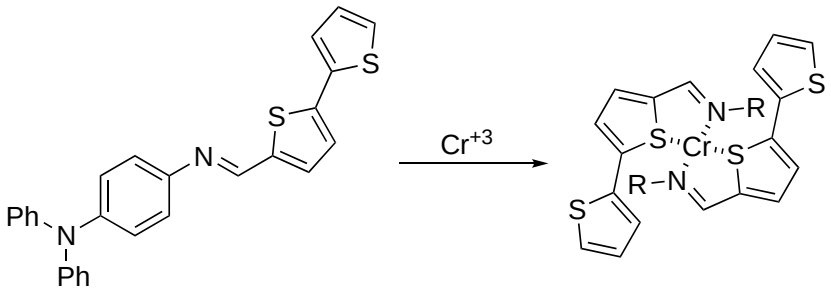

Non-fluorescent Fluorescent

Scheme 3. Binding mode of Schiff base derivative with Cr (III) ions.

In 2023, Singh G. *et al.* synthesized a *p*-rosolic acid derivative containing 1,2,3-triazole moieties (**Scheme 4**). This probe was able to detect Hg (II), Pb (II) and Cr (III) ions by inhibition of PET mechanism. The LOD calculated for Cr (III) was 0.12 μM and the binding stoichiometry was found to be 1:1 (36).

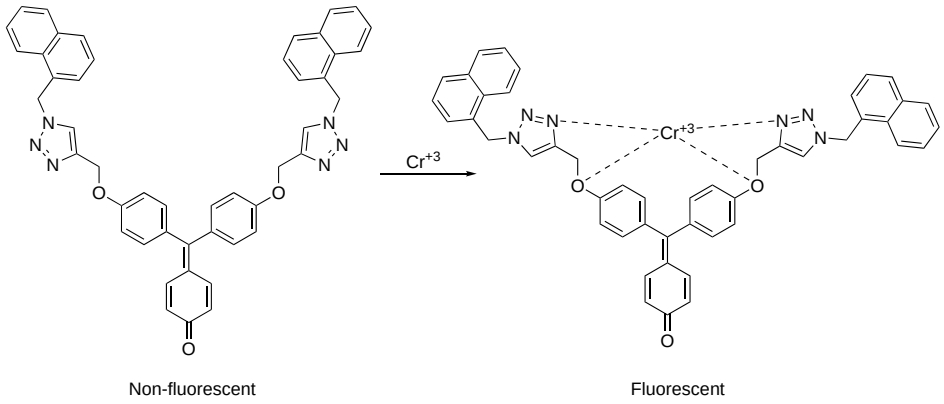

Scheme 4. Binding mode of *p*-rosolic acid derivative with Cr (III) ions.

In 2023, Liu Y. *et al.* synthesized an oxazole derivative that presents “off-on-off” fluorescence (**Scheme 5**). This compound in its free state shows fluoresce (Φ=0.08) and, upon coordination with In (III), a sharp enhancement of fluorescence is observed at 512 nm (Φ=0.71). Other metal ions did not enhance the fluorescence of the compound, but when interferences were tested, it was seen that Cr (III) quenches the fluorescence due to a preferable binding. This compound was then tested as an In (III) sensor with subsequent use as Cr (III) sensor. The binding stoichiometry for both compounds was found to be 1:2 with LODs of 6.21×10^{-10} M and 9.82×10^{-9} M, respectively for In (III) and Cr (III) ions (37).

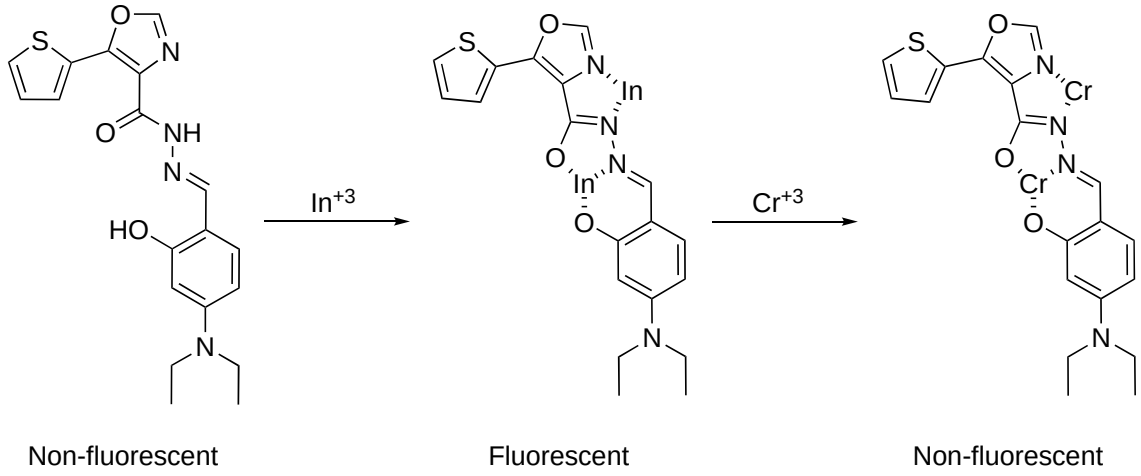

Scheme 5. Binding mode of oxazole derivative with In (III) and Cr (III) ions.

Furthermore, azole moieties like oxadiazole and triazole have been used in the construction of many colorimetric and fluorometric sensors for other metal ions. These heterocycles contain free pair of electrons that can coordinate to the metal ions, hence being good candidates as fluorophores or ionophores. **Table 2** summarizes some reports of oxadiazole, triazole and benzotriazole derivatives that can selectively sense different heavy metal ions. Most of these metal ion sensors could selectively sense different metal ions with no interferents reported. The LOD of most of these sensors are in the μM range, thus being reliable to determine trace level concentrations in samples.

Table 2. Summary of sensors where oxadiazole, triazole, and benzotriazole have been used.

Sensor structure	Metal	Interferences	Technique	LOD (μM)	Lineal Range	Ref.
Oxadiazole	Ag^{+}	N/A	UV-Vis	9.784	0-0.419 mM	(38)
	Co^{2+}			28.34	0-0.348 mM	
	Cu^{2+}			8.533	0-0.411 mM	
	Pd^{2+}	N/A	PL	0.00397	0.1 - 1 μM	(39)
	Fe^{2+}	N/A	PL	7.78	30-300μM	(40)
	Fe^{3+}			6.95	30-300μM	
	Fe^{2+}	N/A	PL	2.977	1-8 μM	(41)
	Ni^{2+}			0.895	1-8 μM	
	Cu^{2+}			0.593	1-8 μM	
	Hg^{2+}	N/A	UV-Vis	No report	No report	(42)
			PL			
Triazole	Au^{3+}	Hg^{2+}	PL	0.08	0-0.34 mM	(43)
	Cu^{2+}	N/A	UV-Vis	0.12	1-100 μM	(44)
	Fe^{2+}			0.11	1-100 μM	
	Sn^{2+}	N/A	UV-Vis	0.047	0.2-0.9μM	(45)
			PL	0.0038	5 – 30 nM	
	Hg^{2+}	N/A	PL	0.13	0-400 μM	(46)
	Cu^{2+}	N/A	PL	1.24	0-50 μM	(47)
			UV-Vis	3.7	0-20 μM	
	Pb^{2+}		PL	0.99	0-50 μM	
			UV-Vis	1.2	0-30 μM	
Benzotriazole	Zn^{2+}	N/A	PL	0.0028	0-12 μM	(48)
	Cu^{2+}	N/A	PL	0.0144	0-50 μM	(49)
	Cu^{2+}	N/A	PL	300	0-1.5 mM	(50)

2.2 Synthesis

Synthetic methods to obtain carboxylic acid and oxadiazole moieties were researched. Carboxylic acid can be obtained by different methods such as oxidation of primary alcohol (51); hydrolysis of nitriles, esters, anhydrides, etc. (52); and carboxylation with CO_2 (53) (**Scheme 6**). Conversely, oxadiazole can be synthesized by cyclocondensation using hydrazides and carboxylic acids (54), Huisgen's rearrangement using tetrazoles and activated carboxylic acids (55), oxidative cyclization of hydrazones (56), and dehydrative cyclization of diacyl hydrazides (57) (**Scheme 7**).

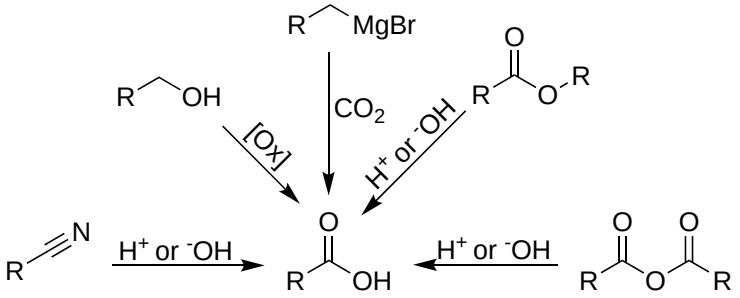

Scheme 6. Different approaches to obtain carboxylic acid.

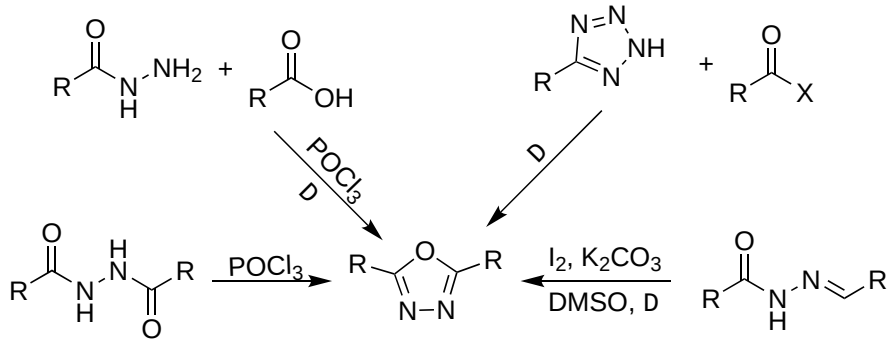

Scheme 7. Different approaches to obtain oxadiazole.

The research group has published the synthesis of fluorescent benzotriazole derivatives containing ethyl ester (58) and nitrile (59) moieties for cell imaging (**Figure 7**). Hence, these reports were used as inspiration for the design and synthesis for compounds **BTZ-COOH** and **BTZ-O**. Thus, hydrolysis of an ester

group and Huisgen's rearrangement were chosen as the best options to synthesize the target compounds.

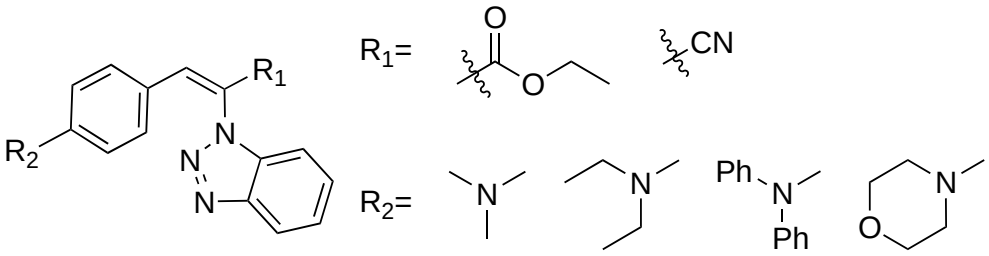

Figure 7. Fluorescent benzotriazole derivatives synthesized by the research group.

2.3 Critical Analysis

As can be seen from the state-of-the-art analysis, Cr (III) ions have been selectively sensed using fluorescence spectroscopy with organic molecules. The organic molecules used to quantify this metal contain functional groups with nitrogen atoms (amine, imine, pyridine and triazole), oxygen atoms (carboxylic acid, furan, alcohol, carbonyl), or both (oxazole), demonstrating the affinity of these functional groups to Cr (III) ions. Benzotriazole and oxadiazole have not been used to sense Cr (III) ions but are great candidates due them having lone pair of electrons that can coordinate with metal ions.

2.4 Hypothesis

Al least one of the benzotriazolyl vinyl aniline derivatives sense Cr (III) using UV-Vis or PL spectroscopy with a LOD < 0.1 μM.

2.5 Objectives

2.5.1 General Objective

To synthesize two new benzotriazolyl vinyl aniline derivatives, determine their structure and photophysical properties and apply them as metal ion sensors in solution.

2.5.2 Specific Objectives

- To synthesize ethyl benzotriazolyl acetate **2** by ultrasonic bath.
- To synthesize ethyl benzotriazolyl acrylate **3** by Knoevenagel's condensation.
- To synthesize benzotriazolyl acrylic acid **BTZ-COOH** by ultrasound irradiation assisted hydrolysis.
- To synthesize benzotriazolyl-acetonitrile **4** by ultrasonic bath.
- To synthesize benzotriazolyl-acrylonitrile **5** by Knoevenagel's condensation.
- To synthesize benzotriazolyl-tetrazole **6** by Huisgen's cycloaddition.
- To synthesize α,β-unsaturated benzotriazolyl-oxadiazole **BTZ-O** by Huisgen's rearrangement.
- To characterize all compounds by FT-IR, ^{1}H-NMR, ^{13}C-NMR, and HRMS to elucidate their structure.
- To characterize the photophysical properties of compounds **BTZ-X** by UV-Vis and PL spectroscopies.
- To evaluate the change in photophysical properties of the compounds **BTZ-X** in solution with different metal ions by UV-Vis and PL spectroscopies.
- To evaluate the possible interferences in the detection of Cr (III).
- To evaluate the stoichiometric ratio between **BTZ-X** and Cr (III).
- To evaluate the lineal range and limit of detection for Cr (III) with **BTZ-X**.

3 Materials and Methods

3.1 Instruments

The synthesis of the organic compounds was done in Laboratorio de Química Industrial (CELAES-FCQ-UANL). The equipment used from this facility includes: an Anton Paar Monowave 300 microwave reactor, a Branson 5510 ultrasound bath. Electrothermal Mel-Temp apparatus was used to register the melting points and were uncorrected. Thin layer chromatography (TLC) plates were revealed using Spectroline UV lamps at 254 and 365 nm.

The structural elucidation was carried out in the following Laboratories: Nuclear Magnetic Resonance, Bruker 700 MHz (CIBYN-FCQ-UANL) and Bruker 500 MHz (BYU); Infrared Spectroscopy, Perkin Elmer Spectrum-One (Laboratorio de Análisis Instrumental FCQ-UANL); and HRMS, Agilent, 6210 TOF (BYU).

For the photophysical characterization a Mettler Toledo UV5 spectrophotometer was used to record UV-Vis absorption spectra and a Perkin-Elmer PL-8500 fluorescence spectrophotometer was used to record emission spectra. Both instruments are in Laboratorio 4 de Química Orgánica (FCQ-UANL).

3.2 Reagents

The reagents used for all the experiments are described in **Table 3**.

Table 3. List of reagents and suppliers.

Supplier	Reagents
Sigma Aldrich	Benzotriazole 99%, ethyl bromoacetate 98%, chloroacetonitrile 98% piperidine 99%, 4-dimethylaminobenzaldehyde 99%, lithium hydroxide 98%, potassium azide 99%.
Desarrollo de Especialidades Químicas	Potassium carbonate (K_2CO_3), anhydrous sodium sulfate (Na_2SO_4), sodium bicarbonate ($NaHCO_3$). Reagent grade solvents: acetonitrile, toluene, ethanol, water, ethyl ether. Industrial grade solvents: hexane, ethyl acetate, methanol, acetone.

3.3 Synthetic methodology

*3.3.1 Synthesis of ethyl benzotriazolyl acetate **2***

In a round bottom flask, 1.0 eq (5 g) of benzotriazole, 2.2 eq of K_2CO_3 and 50 mL of acetonitrile were added and then 1.2 eq of ethyl bromoacetate was added dropwise. The mixture was positioned in an ultrasonic bath at 50 ºC for 4 h and was monitored by TLC using hexane: ethyl acetate (Hex:EtOAc) at a ratio of 7:3 v/v. After the reaction was done, 30 mL of distilled water was added to the flask and extracted with ethyl acetate three times with 20 mL (3 x 20 mL), the organic layer was dried with anhydrous sodium sulfate, filtered and vacuum distilled. The crude solid was purified by column chromatography using silica gel as stationary phase and Hex:EtOAc (7:3 v/v) as mobile phase.

*3.3.2 Synthesis of ethyl benzotriazolyl acrylate **3***

In a G-10 microwave vessel, provided with magnetic stirring, 1.0 eq (0.5 g) of compound **2**, 1.2 eq of *p*-(dimethylamino) benzaldehyde, 2.0 eq of piperidine, and 3.5 mL of anhydrous ethanol were added. The mixture was heated for 60 min at 100 ºC under MW irradiation. The reaction progress was monitored by TLC using Hex:EtOAc (7:3 v/v). When the reaction was done, the mixture was cooled to room temperature and a solid was filtered and washed with cooled diethyl ether and dried.

*3.3.3 Synthesis of benzotriazolyl acrylic acid **BTZ-COOH***

In a round bottom flask, 1.0 eq (0.5 g) of compound **3**, 3 eq of LiOH, and 4 mL of MeOH:H_2O (3:1 v/v) mixture were added. The reaction mixture was placed in an ultrasonic bath at 50 ºC for 4 h. The reaction progress was monitored by TLC using Hex:EtOAc (7:3 v/v). After the reaction is completed, the mixture was vacuumed distilled, and 30 mL of distilled water was added to the flask. The resulting mixture was extracted with ethyl acetate three times with 20 mL (3 x 20

mL). The aqueous layer was acidified with conc. HCl until a precipitate is formed. The solid was filtered, washed with distilled water, and dried.

*3.3.4 Synthesis of benzotriazolyl acetonitrile **4***

In a round bottom flask, 1.0 eq (5 g) of benzotriazole, 2.2 eq of K_2CO_3, and 50 mL of acetonitrile were added and then 1.2 eq of chloroacetonitrile was added dropwise. The mixture was positioned in an ultrasonic bath at 50 ºC for 4 h was monitored by TLC using Hex:EtOAc (7:3 v/v). After the reaction was done, 30 mL of distilled water was added to the flask extracted with ethyl acetate (3 x 20 mL), the organic layer was dried with anhydrous sodium sulfate, filtered and vacuum distilled. The crude solid was purified by column chromatography using silica gel as stationary phase and Hex:EtOAc (7:3 v/v) as mobile phase.

*3.3.5 Synthesis of benzotriazolyl acrylonitrile **5***

In a G-10 microwave vessel, provided with magnetic stirring, 1.0 eq (0.5 g) of compound **4**, 1.2 eq of *p*-(dimethylamino) benzaldehyde, 2.0 eq of piperidine, and 3.5 mL of anhydrous ethanol were added. The resulting mixture was heated at 100 ºC for 60 min under microwave irradiation with constant stirring. The reaction progress was monitored by TLC using Hex:EtOAc (7:3 v/v). The reaction mixture was cooled to room temperature and the solid product was filtered and washed with cooled diethyl ether and dried.

*3.3.6 Synthesis of benzotriazolyl tetrazole **6***

In a G-30 microwave vessel, provided with magnetic stirring, 1.0 eq (0.5 g) of compound **5**, 2.0 eq of potassium azide (KN_3), and 10 mL of *N*-methylpyrrolidone: acetic acid: water (NMP:AcOH:H_2O) at a ratio of 5:2:3 v/v were added. The resulting mixture was heated at 160 ºC for 70 min under microwave irradiation with constant stirring. The reaction progress was monitored by TLC using Hex:EtOAc (7:3 v/v). The reaction mixture was cooled to room temperature, then transferred to a beaker. Sodium bicarbonate ($NaHCO_3$) was added to the reaction

mixture to neutralize the solution. The resulting mixture was extracted once with 30 mL of ethyl acetate. The aqueous layer was acidified with conc. HCl until a precipitate is formed. The solid was then be filtered, washed with distilled water, and dried.

*3.3.7 Synthesis of α,β-unsaturated benzotriazolyl oxadiazole **BTZ-O***

In a G-30 microwave vessel, 1.0 eq (0.5 g) of compound **6,** 1.5 eq of benzoic acid, 1.5 eq of *N,N'*-dicyclohexylcarbodiimide (DCC), and 10 mL of toluene were added. The resulting mixture was heated at 140 ºC for 60 min under microwave irradiation with constant stirring. The reaction progress was monitored by TLC using Hex:EtOAc (7:3 v/v). After the reaction is completed, the solvent was vacuum distilled, and 5 mL of methanol was added to dissolve by-products. The mixture is then filtered and washed with cooled diethyl ether and afterwards dried.

*3.3.8 Synthesis of benzotriazolyl acetic acid **7***

In a round bottom flask, 1.0 eq (0.5 g) of compound **2**, 3 eq of LiOH, and 4 mL of MeOH:H_2O (3:1 v/v) mixture were added. The mixture was positioned in an ultrasonic bath at 50 ºC for 4 h and monitored by TLC using Hex:EtOAc (7:3 v/v). After the reaction was done, the mixture was vacuumed distilled, and 30 mL of distilled water was added to the flask and extracted with ethyl acetate (3 x 20 mL). The aqueous layer was acidified with conc. HCl until a solid was formed. The solid was filtered, washed with water, and dried.

*3.3.9 Synthesis of phenyl tetrazole **9***

In a round bottom flask, 1.0 eq (1g) of benzonitrile, 1.1 eq of NaN_3, 1.1 eq of NH_4Cl, and 20 mL of DMF were added. The reaction mixture was heated at 120 ºC for 24 h with strong stirring. The reaction progress was monitored by TLC using Hex:EtOAc (7:3 v/v). After the reaction was completed, the mixture poured into 200 mL of ice-cold distilled water. The resulting mixture was acidified with

conc. HCl until a solid precipitated is formed. The solid was then filtered, washed with distilled water, and dried under vacuum.

*3.3.10 Synthesis of benzotriazolyl oxadiazole **10***

In a round bottom flask, 1.0 eq (0.5g) of compound **7**, 1.1 eq of DCC and 10 mL of dry toluene were stirred at room temperature for 30 min under Ar atm, then 1.1 eq of compound **8** was added. The reaction mixture was heated at 90 ºC for 24 h with strong stirring and under Ar atm. The reaction progress was monitored by TLC using Hex:EtOAc (7:3 v/v). After the reaction was completed, the mixture was vacuum distilled and 20 mL of EtOAc were added. The crude mixture was cooled in the fridge overnight and later filtered. The liquor was then concentrated and allowed to cool in the fridge, and later filtered until no more solid precipitated.

*3.3.11 Alternative synthesis of **BTZ-O***

In a G-10 microwave vessel, provided with magnetic stirring, 1.0 eq (0.4474 g) of compound **9**, 1.2 eq of *p*-(dimethylamino) benzaldehyde, 2.0 eq of piperidine, and 3.5 mL of anhydrous ethanol were added. The resulting mixture was heated at 100 ºC for 60 min under microwave irradiation with constant stirring. The reaction progress was monitored by TLC using Hex:EtOAc (7:3 v/v). The reaction mixture was cooled to room temperature and the solid product was filtered and washed with cooled diethyl ether and dried.

3.4 Metal sensing

3.4.1 Photophysical properties

For the measurement of the photophysical properties, 10 mg of compound **BTZ-X** were dissolved in 10 mL of the appropriate solvent to obtain a stock solution of 1000 ppm. Then 20 ppm dilutions were prepared and analyzed by UV-Vis spectroscopy. A solution with A > 0.1 was prepared and analyzed by PL spectroscopy. Maximum absorption, emission and excitation wavelengths, and absorbance were recorded for all compounds.

3.4.2 Metal ion selectivity assay

To 4 mL of a 10 μM solution of ligand **BTZ-X** in the appropriate solvent were added 100 μL of a 2 mM metal ion solution in deionized water. One mixture was prepared per metal ion. The mixtures were stirred and left to rest 30 min and measured by UV-Vis and PL spectroscopies. The data was collected and compared with a control solution and the other metals, to determine the one with the higher shift, quenching or enhancement in their photophysical properties.

3.4.3 Cr (III) interference tests

To 4 mL of a 10 μM solution of ligand **BTZ-X** were added 100 μL of mixtures of Cr(III) and different metal ions both at a concentration of 2 mM. One mixture was prepared per additional metal ion. The mixture was stirred and left to rest 30 min and measured by UV-Vis and PL spectroscopies. The data was collected and compared with a control solution to determine the possible interferences.

3.4.4 Job's Plot

5 mL of solutions containing varying molar fractions of ligand **BTZ-X** and Cr(III) with a total concentration of 10 μM were prepared. These solutions were left to rest 30 min and measured by UV-Vis and PL spectroscopies. The data was collected, and the area of the emission band was plotted against the molar fraction to determine the ligand to metal ratio.

3.4.5 Linear range and limit of detection

Mixtures of 4 mL of 10 μM ligand and 100 μL of Cr (III) in increasing concentration were stirred and left to rest 30 min and measured by UV-Vis and PL spectroscopies. The data was collected and compared with a control solution; the area of the emission band was plotted against the metal ion concentration. The (LOD) was calculated using **Eq. 1**, where m is the slope of the linear correlation curve and s_B is the standard deviation of the blank.

$$LOD = 3s_B/m \qquad \textbf{Eq. 1}$$

3.5 Waste Disposal

Waste management and disposal was done in accordance with the regulations of the Departamento de Medio Ambiente y Seguridad (FCQ-UANL).

Table 4. Waste disposal chart.

Residue	Container
Aqueous solutions	A
Inorganic solids	B
Organic non-halogenated solutions	C
Organic halogenated solutions	D
Toxic, carcinogenic organic solutions	E_{org}
Toxic, carcinogenic inorganic solutions	E_{inorg}
Precious metal solutions	F
Organic solids	G
Oxidants	H
Absorbent materials that were in contact with chemicals, latex gloves	Industrial waste
Empty glassware that was in contact with chemicals	Impregnated glass
Empty plastic material that was in contact with chemical substances	Impregnated plastics

4 Results and Discussion

4.1 Organic Synthesis

*4.1.1 Synthesis of benzotriazolyl acrylic acid **BTZ-COOH***

The synthesis of **BTZ-COOH** followed a three-step reaction process as shown in **Scheme 8**. First, ethyl benzotriazolyl acetate **2** was synthesized by a S_N2 reaction assisted by ultrasound between benzotriazole and ethyl bromoacetate. Secondly, compound **2** and p-(dimethylamino)benzaldehyde reacted in a Knoevenagel condensation assisted by MW irradiation to afford ethyl benzotriazolyl acrylate **3**. Finally, compound **3** was hydrolyzed with LiOH to obtain **BTZ-COOH**.

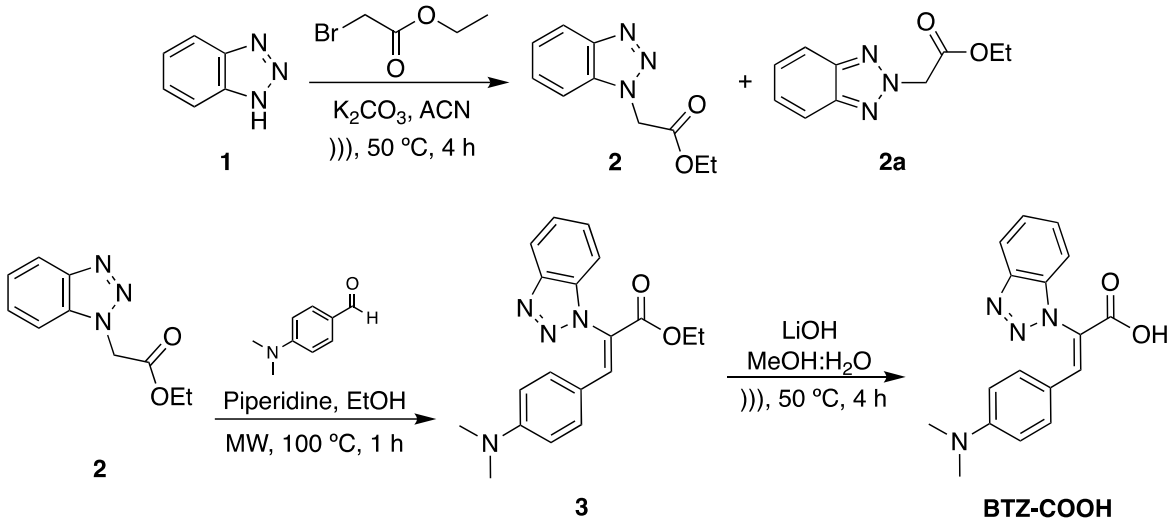

Scheme 8. Synthetic route to obtain **BTZ-COOH**.

4.1.1.1 Ethyl benzotriazolyl acetate **2**

For the synthesis of ethyl benzotriazolyl acetate **2**, a mixture of benzotriazole, ethyl bromoacetate, K_2CO_3, and acetonitrile were sonicated at 50 ºC for 4 h (**Scheme 9**).

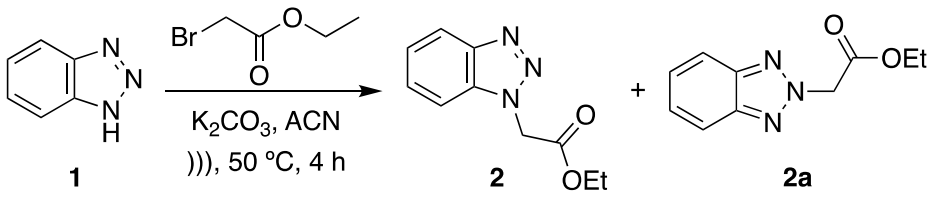

Scheme 9. *N*-alkylation to obtain ethyl benzotriazolyl acetate **2**.

This reaction produces two products, attributed entirely to the tautomeric nature of benzotriazole in solution. In solution benzotriazole can be found in two forms, the *1H*- and *2H*-isomer as shown in **Figure 8**. Even though both isomers can be found in solution, the *1H*-isomer is the most stable, hence it is more readily available to react and leads to a greater yield of the *1H*-isomer.

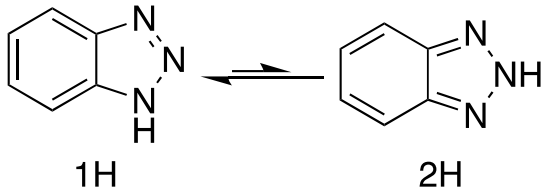

Figure 8. Tautomerization of benzotriazole in solution.

After the reaction was completed, 30 mL of distilled water was added to the crude product and the resulting solution was extracted with EtOAc (3 x 20 mL). The organic layer was dried and vacuum distilled. The resulting oil was then purified by column chromatography on silica gel, using Hex:EtOAc (7:3 v/v) as eluent. Both benzotriazolyl-acetate isomers were separated with column chromatography, being compound **2a** the first to elute. Compounds **2** and **2a** were obtained with chemical yields of 88% and 12% respectively.

The products were structurally characterized and easily distinguished by NMR spectroscopy. The ^{1}H-NMR spectra of both compounds (**Figure 9**) share some similarities; the presence of a triplet (3 H) and quartet signal (2 H), characteristic of an ethyl group and the presence of a singlet signal (2 H) due to the methylene group between the benzotriazole and carbonyl groups. The key difference that can distinguish both products is in the aromatic region (6-8 ppm), where the *1H*-

isomer presents four signals and the *2H*-isomer only two signals. This difference in the number of signals is due to the local symmetry in the benzotriazole ring of compound **2a**, making the hydrogens equal.

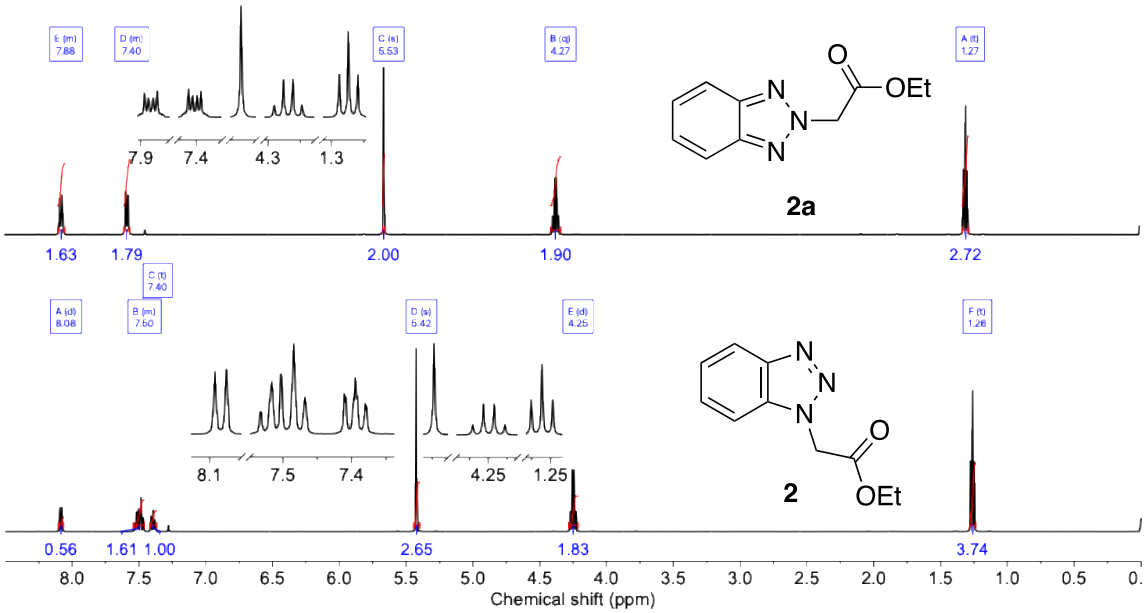

Figure 9. ^{1}H-NMR spectra of compounds **2** and **2a** in $CDCl_3$.

4.1.1.2 Ethyl benzotriazolyl acrylate **3**

For the synthesis of ethyl benzotriazolyl acrylate **3**, a mixture of compound **2**, *p*-(dimethylamino) benzaldehyde, piperidine, and anhydrous ethanol was heated under microwave irradiation at 100 ºC for 60 min (**Scheme 10**).

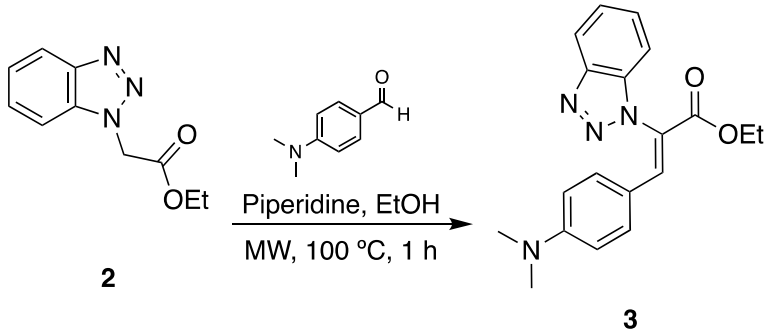

Scheme 10. Knoevenagel condensation to obtain ethyl benzotriazolyl acrylate **3** by MW.

After the reaction time was done, the crude reaction was left to cool down in the refrigerator overnight. Then, a yellow-orange precipitate was vacuum filtered, washed with cold ethyl ether and left to dry. The chemical yield for compound **3** was 35%.

For this reaction, the condensation of the *p*-(dimethylamino)benzaldehyde and the corresponding ethyl benzotriazolyl acetate can be observed by NMR spectroscopy, as shown in **Figure 10**. The singlet of the methylene hydrogens at 5.42 ppm of the ethyl benzotriazolyl acetate disappears due to the condensation in that position. The presence of the aldehyde can be deduced by the singlet (6 H) at 2.91 ppm from the dimethyl amine group and a singlet (1 H) at 8.11 ppm due to the formed vinylic bond. Also, in the aromatic region, two doublets (2 H, J=9.1 Hz), at 6.36 and 6.58 ppm, correspond to the *p*-substituted benzene from the aldehyde. Additionally, the ethyl group signals from the reactant are still present, suggesting that the ester group did not react.

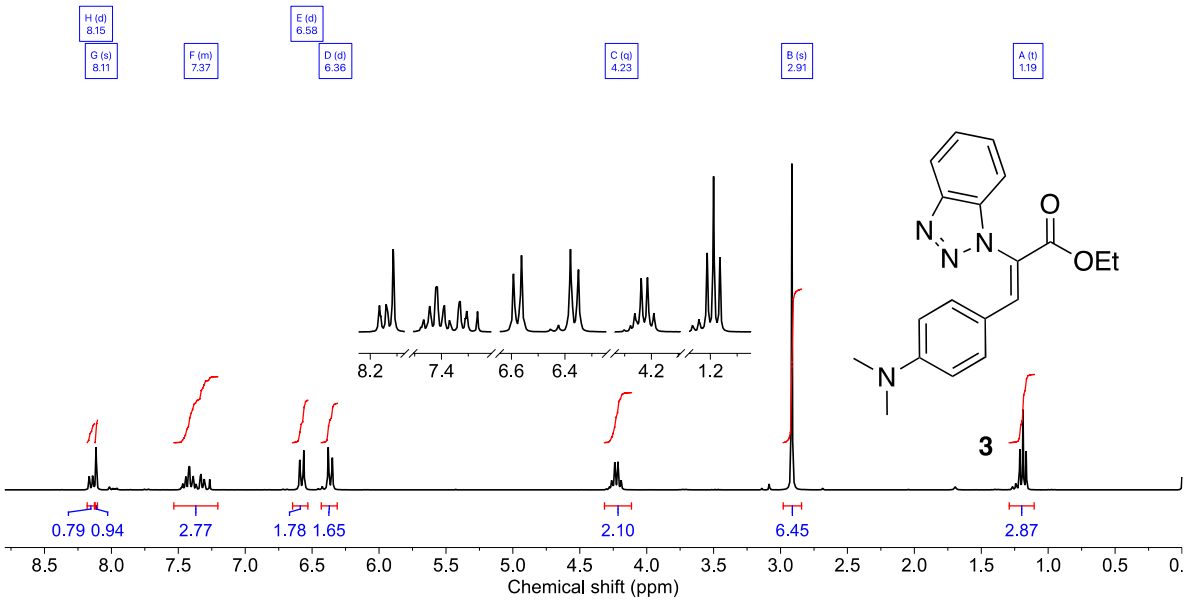

Figure 10. ^{1}H-NMR spectrum of compound **3** in $CDCl_3$.

4.1.1.3 **BTZ-COOH**

For the synthesis of **BTZ-COOH**, compound **3** and LiOH were dissolved in a MeOH:H_2O mixture (3:1 v/v). The resulting mixture was left to react under ultrasound irradiation at 50 ºC for 4 h (**Scheme 11**).

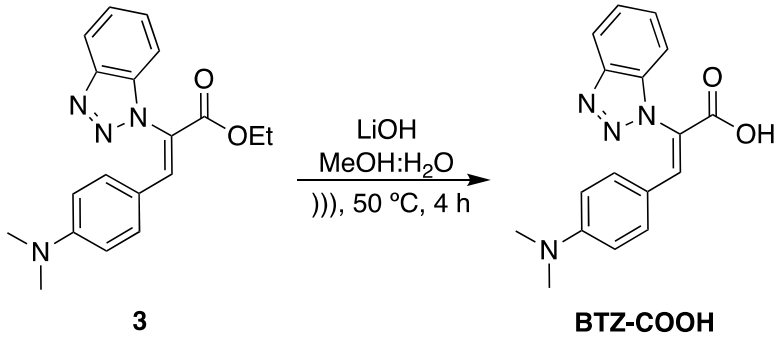

Scheme 11. Hydrolysis to obtain **BTZ-COOH**.

After the reaction time, the mixture was vacuum distilled to remove the MeOH and extractions with EtOAc were done to remove the remaining reactant. Afterwards, the aqueous layer was acidified with conc. HCl until a precipitate formed. This yellow solid was filtered, washed with distilled water, and dried. The chemical yield for **BTZ-COOH** was 74%.

The NMR spectrum for both compounds, **3** (**Figure 10**) and **BTZ-COOH** (**Figure 11**), look similar. The same signals are present for the dimethyl amine group, the vinylic bond, and the aromatic rings in both compounds. The key difference to determine a successful reaction is the disappearance of the triplet and quartet signals of the ethyl ester, which should have been hydrolyzed during the reaction.

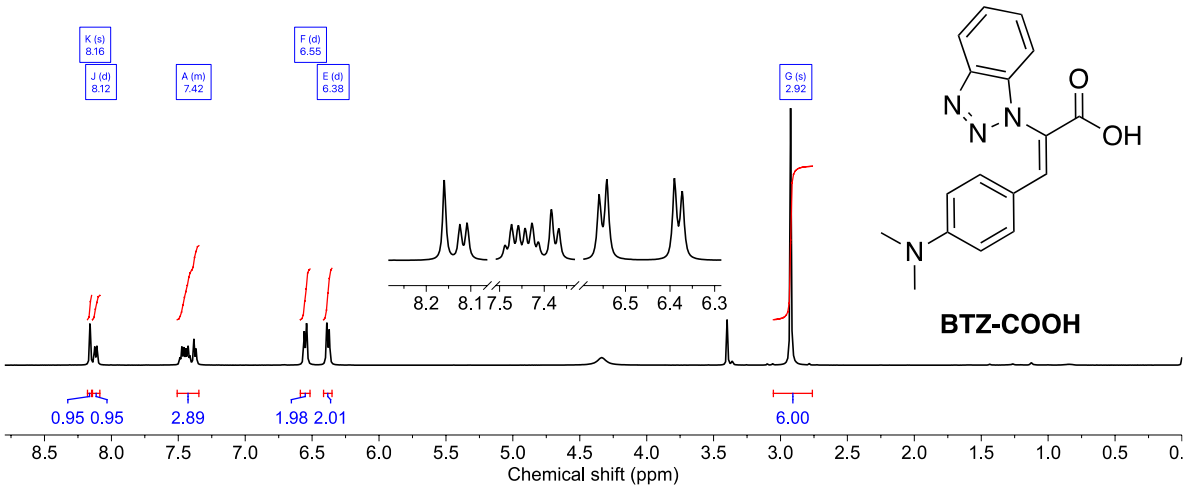

Figure 11. ^{1}H-NMR spectrum of compound **BTZ-COOH** in $CDCl_3$ and CD_3OD.

*4.1.2 Synthesis of α,β-unsaturated benzotriazolyl oxadiazole **BTZ-O***

The synthesis of **BTZ-O** followed a four-step reaction process as shown in **Scheme 12**. First, benzotriazolyl acetonitrile **4** was synthesized by a S_N2 reaction assisted by ultrasound between benzotriazole **1** and chloroacetonitrile. Secondly, benzotriazolyl acetonitrile **4** and *p*-(dimethylamino)benzaldehyde reacted in a Knoevenagel condensation assisted by MW irradiation to form benzotriazolyl acrylonitrile **5**. Then, compound **5** reacted with KN_3 in a Huisgen cycloaddition assisted by MW irradiation to form benzotriazolyl-tetrazole **6**. Finally, compound **6** and benzoic acid reacted under MW irradiation to afford **BTZ-O**.

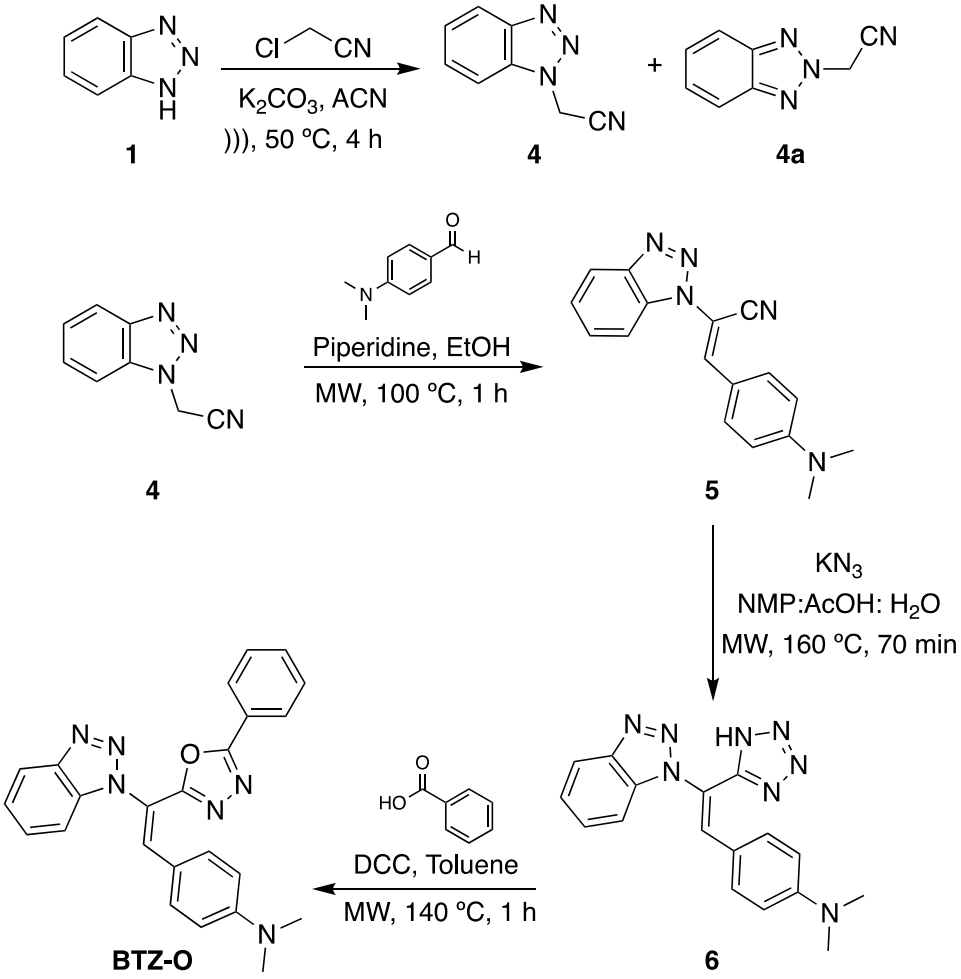

Scheme 12. Synthetic route to obtain compound **BTZ-O**.

4.1.2.1 Benzotriazolyl-acetonitrile **4**

For the synthesis of benzotriazolyl-acetonitrile **4**, a mixture of benzotriazole, chloroacetonitrile, K_2CO_3, and acetonitrile was sonicated at 50 °C for 4 h (**Scheme 13**).

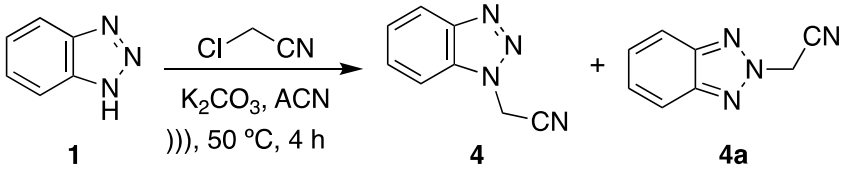

Scheme 13. *N*-alkylation to obtain benzotriazolyl-acetonitrile **4**.

This reaction produces both 1*H* and 2*H*-isomers (compound **4** and **4a** respectively) due to the tautomerization of benzotriazole in solution. Therefore, after the reaction was completed 30 mL of distilled water were added to the crude product and the resulting solution was extracted with EtOAc (3 x 20 mL). The organic layer was dried and vacuum distilled. The resulting oil was then purified by column chromatography on silica gel and Hex:EtOAc (7:3 v/v) as eluent. Both benzotriazolyl-acetonitrile isomers were separated with column chromatography, being compound **4a** the first to elute. Compounds **4** and **4a** were obtained with chemical yields of 75% and 25% respectively. Compound **4** was obtained in greater yield due to the higher stability in solution of 1*H*-isomer compared to the 2*H*-isomer.

The position of the *1H* or *2H* bond can be identified by NMR, as shown in **Figure 12**. The *2H*-isomer, compound **4a**, only presents two multiplet signals corresponding to aromatic hydrogens of the benzotriazole ring, this is attributed to the equivalence of the hydrogens in the benzotriazole group. When benzotriazole is substituted in the *1H* position, compound **4**, equivalence of the aromatic hydrogens is lost, and four sets of signals appear in the spectrum; two doublets that correspond to the hydrogens most near to the triazole ring and two triplets that correspond to the hydrogens furthest from the triazole ring. Furthermore, as can be observed for compounds **4** and **4a**, a singlet that corresponds to the methylene hydrogens is shifted between both spectra, this is due to the stronger shielding effect of the *2H*- benzotriazole in comparison to the *1H*-isomer.

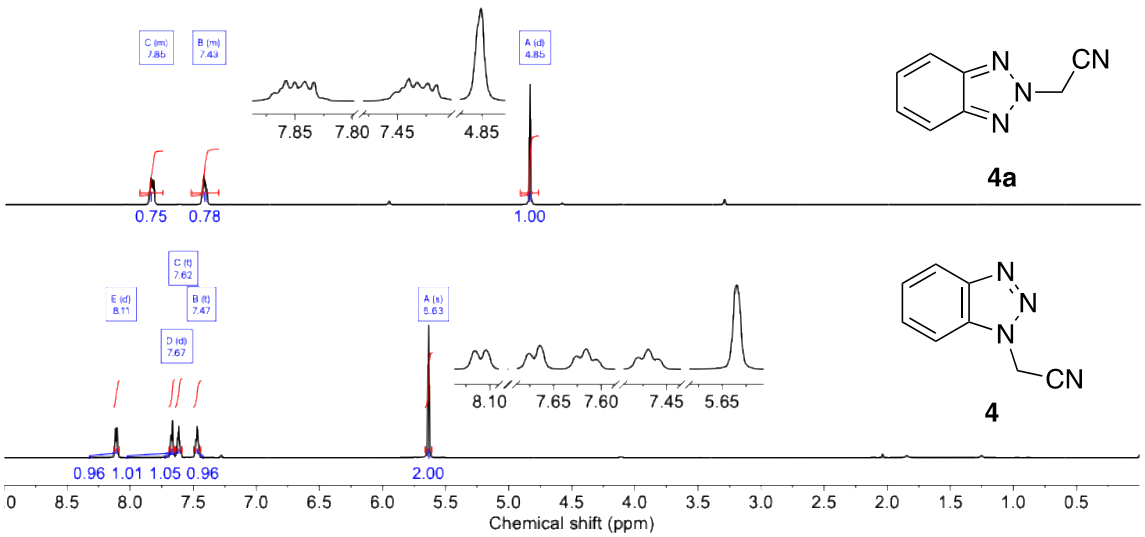

Figure 12. ^{1}H-NMR spectra of compounds **4** and **4a** in $CDCl_3$.

4.1.2.2 Benzotriazolyl acrylonitrile **5**

For the synthesis of benzotriazolyl-acrylonitrile **5**, a mixture of compound **4**, *p*-(dimethylamino) benzaldehyde, piperidine and anhydrous ethanol was heated under microwave irradiation at 100 ºC for 1 h (**Scheme 14**).

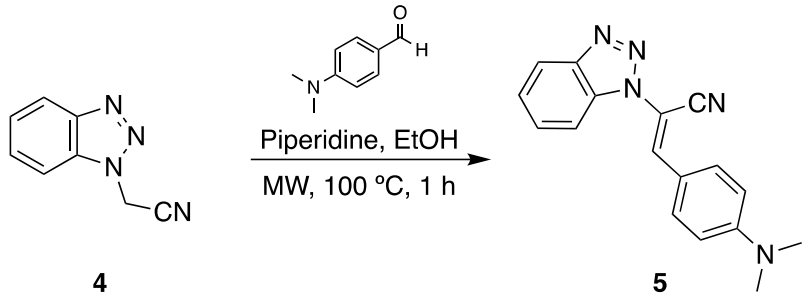

Scheme 14. Knoevenagel condensation to obtain benzotriazolyl acrylonitrile **5**.

After the reaction time, a yellow-orange solid was formed in the reaction vessel. This solid product was filtered and washed with cooled diethyl ether. The solid was obtained with chemical yield of 79%.

For this reaction, the condensation of the *p*-(dimethylamino) benzaldehyde and the corresponding benzotriazolyl-acetonitrile can be observed with NMR, as shown in **Figure 13**. The singlet of the methylene hydrogens of the benzotriazolyl-

acetonitrile at 5.69 ppm disappears due to the formation of the double bond. The presence of the incorporated aldehyde can be deduced by the appearance of a singlet that integrates to six hydrogens at 3.10 ppm approximately; this signal corresponds to the methyl hydrogens of the dimethylamino group. Additionally, in the region of 6-8 ppm one singlet that integrates for one hydrogen and two doublets that integrate for two hydrogens appear. The singlet corresponds to the vinyl hydrogen and both doublets correspond to the hydrogens of the new aromatic ring that was introduced to the molecule.

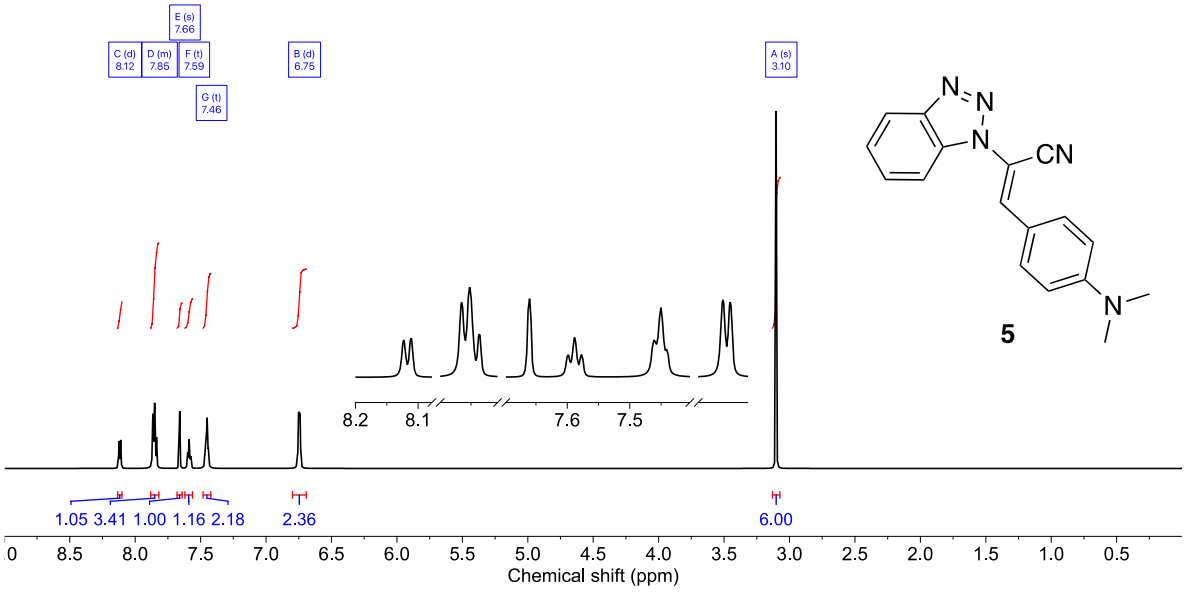

Figure 13. ^{1}H-NMR spectrum of compound **5** in $CDCl_3$.

4.1.2.3 Benzotriazolyl-tetrazole **6**

For the synthesis of benzotriazolyl-tetrazole **6**, a mixture of compound **5**, KN_3 and NMP:AcOH:H_2O (5:2:3 v/v) was heated under microwave irradiation at 160 ºC for 70 min (**Scheme 15**).

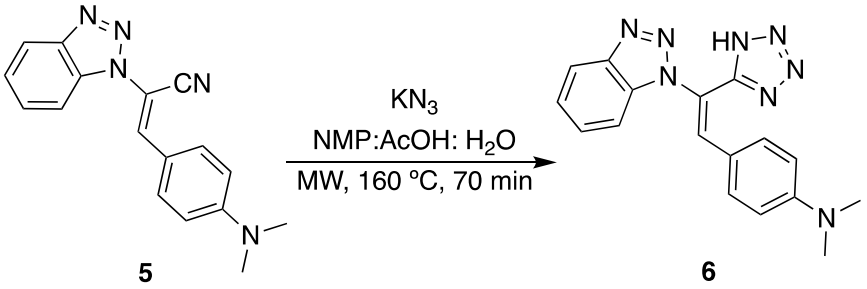

Scheme 15. Huisgen cycloaddition to obtain benzotriazolyl tetrazole **6**.

The crude was transferred to a beaker and the reaction vessel washed with distilled water. Sodium bicarbonate was added to the crude to neutralize the acetic acid in the solution and to dissolve the tetrazole. Extractions with ethyl acetate were done; the product remained dissolved in the aqueous layer. If tetrazole transferred to the organic layer, an extraction with saturated sodium bicarbonate solution was employed. The aqueous layers were acidified with conc. HCl until a precipitate was formed. The solid started to form at pH=5 but stayed suspended. When the pH was lowered between 2 and 3 the solid precipitated. And when an excess of HCl was added (final pH around 1) the solid redissolved. This redissolution may be due to the protonation of one of the nitrogens of the compound. The solid was filtered, washed with distilled water, and dried. The chemical yield for compound **6** was 35%.

For this reaction, the formation of the tetrazole ring shifts the signals of most protons, if compared to the spectrum of the precursor **5**. Not much can be said about the NMR data (**Figure 14**), so HRMS was used to determine if the product was formed or not. With this technique, it was observed that the molecular ion signal agreed to the theoretical value that was expected of the compound.

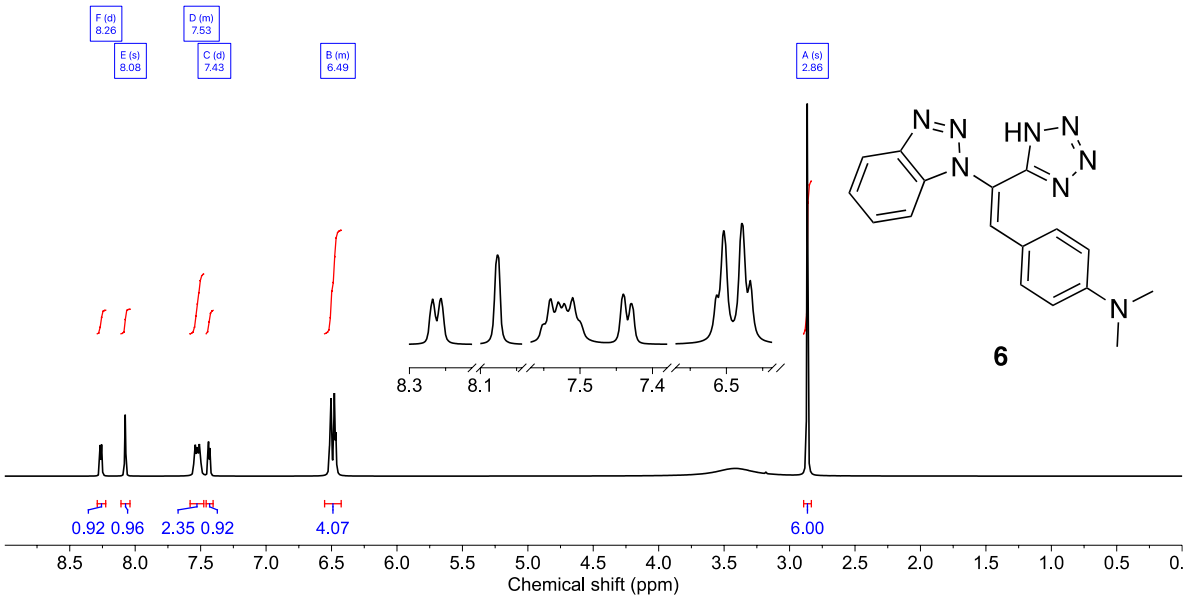

Figure 14. ^{1}H-NMR spectrum of compound **6** in DMSO-d_6.

4.1.2.4 **BTZ-O**

For the synthesis of α,β-unsaturated benzotriazolyl-oxadiazoles **5a** and **5b**, a mixture of compound **4a** or **4b**, benzoic acid, DCC, and toluene was heated at 140 ºC for 1 h under microwave irradiation (**Scheme 16**).

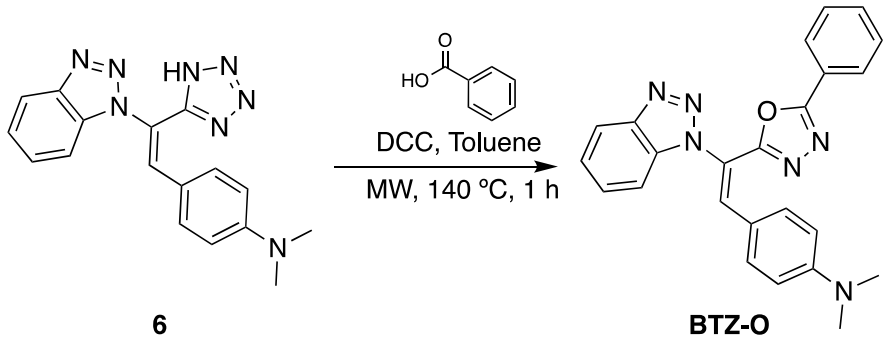

Scheme 16. Huisgen rearrangement to obtain **BTZ-O**.

After the reaction was completed, the toluene was vacuum distilled. 5 mL of methanol was added to the crude solid to dissolve solid by-products, mostly dicyclohexylurea (DCU). The product, **BTZ-O**, was not soluble in methanol thus

filtered, then washed with cooled diethyl ether and dried. The chemical yield of compound **BTZ-O** was 59%.

Figure 15 shows the spectrum of compound **BTZ-O**. If compared to the precursor **6**, the broad singlet around 3.4 ppm disappears, demonstrating that the tetrazole ring reacted with the benzoic acid. Another notorious difference is that in the aromatic region (6-8 ppm) the sum of the hydrogens from the integrals greater by 5 units, these 5 hydrogens come from the aromatic ring of the benzoic acid that was incorporated to the molecule.

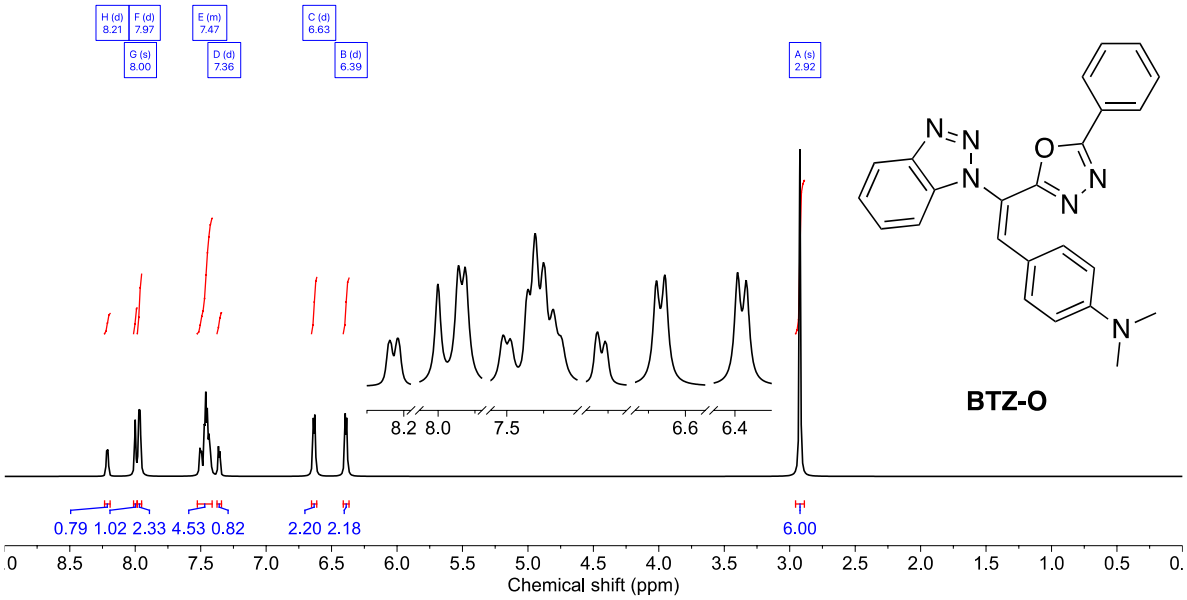

Figure 15. ^{1}H-NMR spectrum of compound **BTZ-O** in $CDCl_3$.

*4.1.3 Alternative synthesis of **BTZ-O***

This alternative route to obtain **BTZ-O** followed a five-step reaction process as shown in **Scheme 17**. The previously synthesized ethyl benzotriazolyl acetate **2** was first hydrolyzed and then reacted with phenyl tetrazole **8** through a Huisgen rearrangement. The obtained benzotriazolyl oxadiazole **10** was then used in a Knoevenagel condensation to afford **BTZ-O** in good chemical yield.

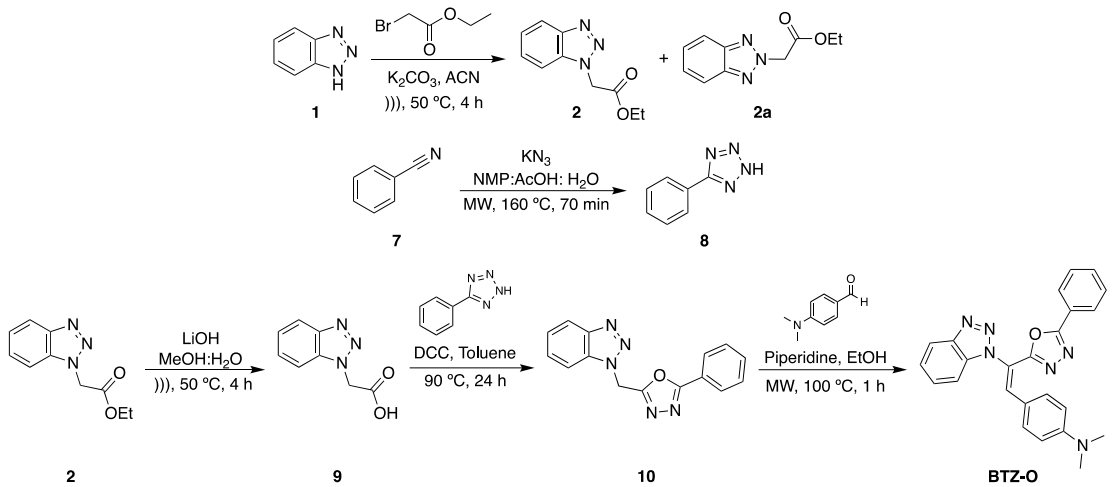

Scheme 17. Alternative synthetic route to obtain compound **BTZ-O**.

As stated in section 4.1.1.1, ethyl benzotriazolyl acetate **2** was successfully synthesized and purified and then hydrolyzed to afford benzotriazolyl acetic acid **7**. Meanwhile, benzonitrile was reacted with KN_3 under a Huisgen cycloaddition to afford the corresponding phenyl tetrazole **8**. Both reactions have been done by the research group and agree with published results found in literature(60,61).

4.1.3.1 Benzotriazolyl oxadiazole **10** and **BTZ-O**

For the synthesis of benzotriazolyl oxadiazole **10**, a mixture of compound **9**, DCC, and toluene was stirred for 30 min under Ar atm. Next, compound **8** was added to the flask and the mixture was allowed to reflux under Ar atm overnight (**Scheme 18**).

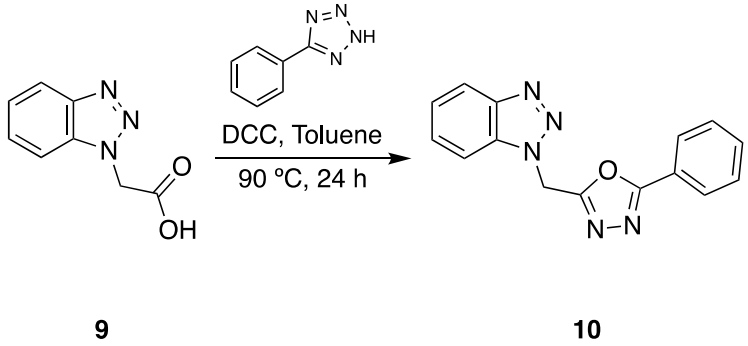

Scheme 18. Huisgen rearrangement to obtain benzotriazolyl oxadiazole **10**.

After the reaction was done, the toluene was vacuumed distilled. The crude solid was dissolved in the least amount of EtOAc and left to cool down in the fridge. When the mixture was cooled a white solid precipitated out of the solution. Said solid was filtered and washed with cold EtOAc. The filtrate was collected and vacuumed distilled.

The solid obtained, thought it had some impurities, was used as is for the next step of the reaction. Compound **10**, *p*-(dimethylamino) benzaldehyde, piperidine, and anhydrous ethanol were heated under microwave irradiation at 100 ºC for 1 h (**Scheme 19**).

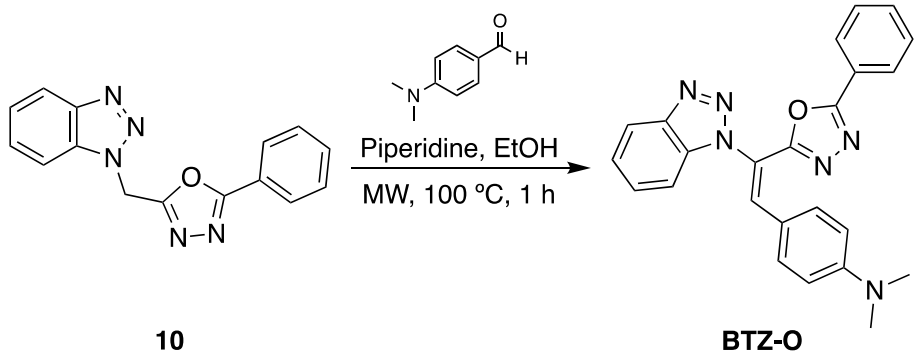

Scheme 19. Knoevenagel condensation to obtain **BTZ-O**.

When the reaction was done and cooled to room temperature, a yellow solid precipitated out of the solution. This solid was filtered and washed with cold diethyl ether. The overall yield between both reactions was 27%.

Figure 16 shows the NMR spectrum of the solid product. In spectrum can be seen two singlets around 2.9 ppm, the one of lowest intensity could be attributed to the presence of the geometric isomer. Comparison of the two spectra (**Figure 15** and **Figure 16**) showed some differences in chemical shifts of the dimethylamine group and the *p*-substituted benzene ring. These changes in chemical shift could be accredited to the obtention of a different geometrical isomer by this method. To prove this difference in geometry, single crystal XRD would be needed.

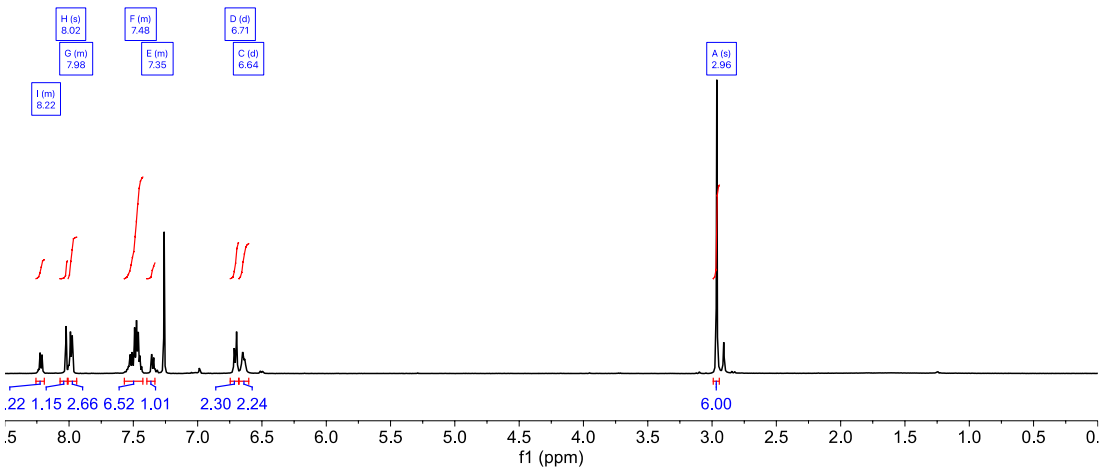

Figure 16. ^{1}H-NMR spectrum of alternate **BTZ-O** in $CDCl_3$.

4.2 Metal Sensing

After both compounds, **BTZ-O** and **BTZ-COOH**, were successfully synthesized and structurally characterized, their photophysical properties were measured and their ability to sense metal ions were studied.

4.2.1 Photophysical Properties

The photophysical properties of both **BTZ-COOH** and **BTZ-O** were measured by UV-Vis and Fluorescence spectroscopies at a concentration of 10 μM and the data is summarized in **Table 5**.

Table 5. Photophysical properties of **BTZ-O** and **BTZ-COOH**.

Compound	Solvent	ε (10^4 $M^{-1}cm^{-1}$)	λ_{abs} (nm)	λ_{em} (nm)	SS (nm)
BTZ-COOH	MeOH	2.83	379	583	204
BTZ-O	ACN	2.92	404	505	101

Figure 17 shows that both compounds exhibit an absorption band with maximum wavelength at 379 and 404 nm, **BTZ-COOH** and **BTZ-O** respectively. These bands can be attributed to the π→π* electronic transition due to the high number

of unsaturated bonds in both molecules. As can be seen in the data, **BTZ-O** has a higher coefficient of extinction and maximum absorption wavelength in comparison to **BTZ-COOH**, this is mainly due to the extra phenyl group in **BTZ-O** that increases the conjugation of the system. On the other hand, as can be seen in the emission spectra and data of both compounds, compound **BTZ-COOH** is red-shifted in comparison to **BTZ-O**. The shift may be due to a more stable delocalization of the electrons in the D-π-A system, which in turn decrease the energy gap between the ground state and excited state.

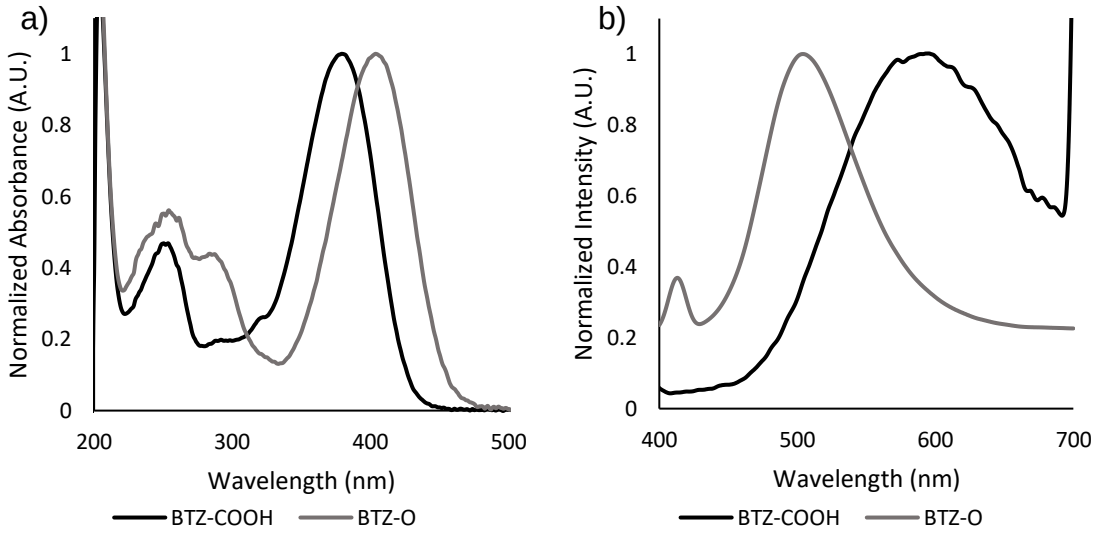

Figure 17. a) UV-Vis spectra and b) fluorescence spectra of **BTZ-COOH** (λ_{ex}=353 nm) and **BTZ-O** (λ_{ex}=413 nm).

4.2.2 Metal ion selectivity essay

Ni^{2+}, Zn^{2+}, Co^{2+}, Cu^{2+}, Mn^{2+}, Pb^{2+}, Cd^{2+}, Al^{3+}, Cr^{3+} and Zr^{4+} ions were used to evaluate the binding properties of compounds **BTZ-COOH** and **BTZ-O** by UV-Vis and fluorescence spectroscopies. In UV-Vis studies, **BTZ-COOH** (**Figure 18a)** shows a bathochromic and hyperchromic shift with most metals, Cr (III) being the one displaying the greatest shift. This effect seen in Cr (III) and other metals might be due to LMCT, where the partially filled HOMO orbitals of the metal lie between the HOMO and LUMO orbitals of the ligand. Excitation will lead to a less energetic promotion of electrons, thus red-shifting the spectrum. On the other hand,

addition of different cations to **BTZ-O** (**Figure 18b**) did not affect the absorption properties of the ligand.

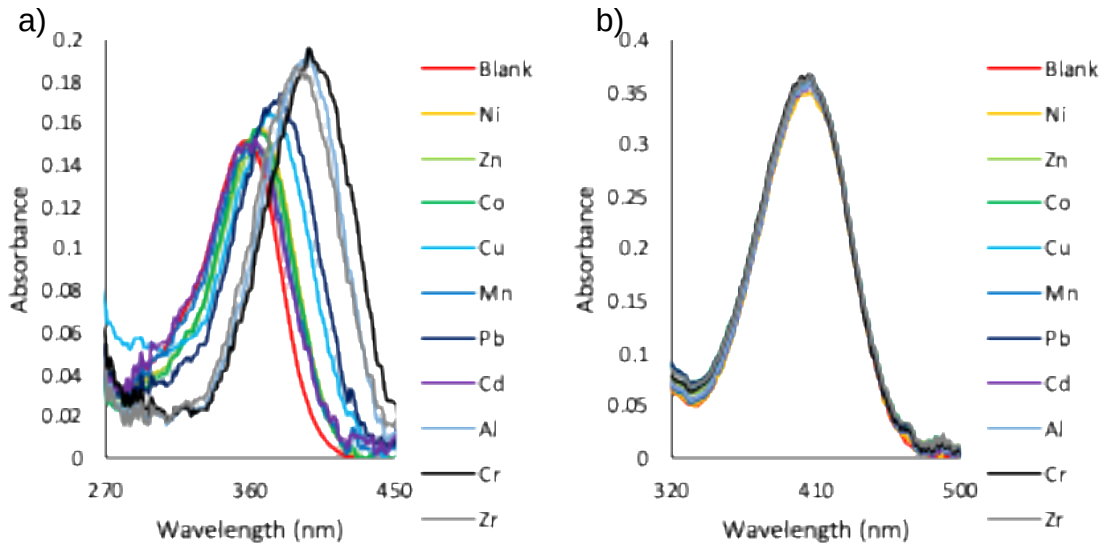

Figure 18. UV-Vis spectra of 4 mL of a) **BTZ-COOH** and b) **BTZ-O** (10 μM) in the presence of 5 eq of different metal ions (100 μL of H_2O).

Fluorescence studies show that **BTZ-COOH** (**Figure 19a**) exhibit various changes in fluorescence intensity with different metal ions. Metals like Cd and Mn increased the fluorescence intensity. Other metals like Al and Zr decreased the fluorescence partially, showing a signal around 500 nm. Cr (III), on the other hand, was selected as the best candidate for sensing applications due to the total quenching of fluorescence. Quenching of the fluorescence intensity can be attributed to an inhibition of fluorescence relaxation by the presence of electrons in the partially filled orbitals of the metal ion. On the other hand, the fluorescence spectra of **BTZ-O** with different metal ions (**Figure 19b**) show that only Cr enhances the inherent fluorescence of the compound. This enhancement could be due to a PET mechanism, where the HOMO orbital of benzotriazole, that is comparable in energy to the fluorophore's orbitals, are stabilized. This stabilization leads to free radiative relaxation between the orbitals of the fluorophore.

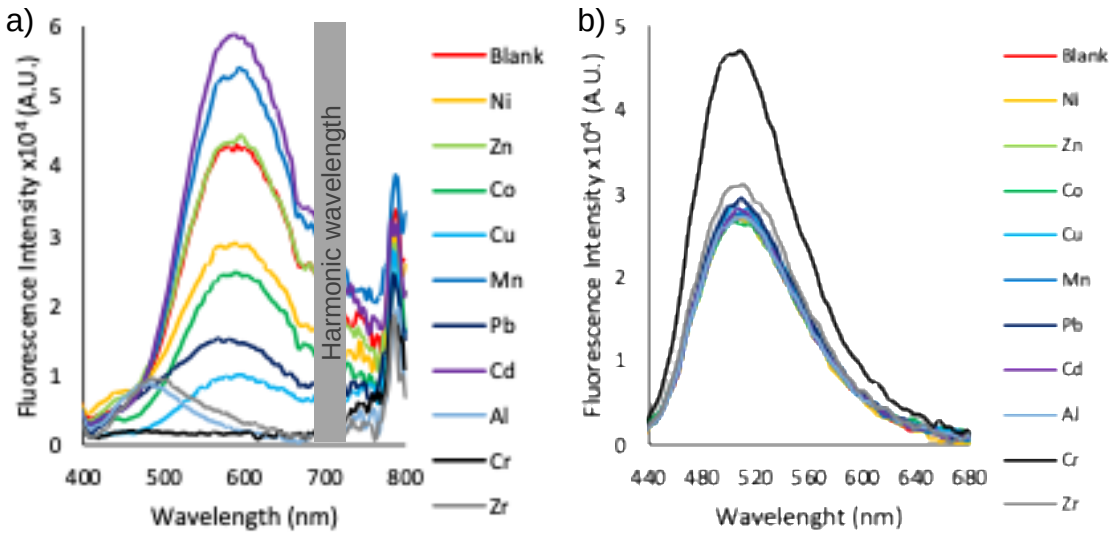

Figure 19. Fluorescence spectra of 4 mL of a) **BTZ-COOH** and b) **BTZ-O** (10 μM) in the presence of 5 eq of different metal ions (100 μL of H_2O). λ_{ex}=353 nm for **BTZ-COOH**, λ_{ex}=413 nm for **BTZ-O**.

For this project, fluorescence spectroscopy was selected as the best spectroscopic technique to sense Cr (III) in solutions due to the large change in fluorescence response, whereas the small bathochromic shift in UV-Vis spectra of **BTZ-COOH** could lead to spectral interferences. Thus, at this stage, part of the hypothesis is approved, due to the ability of both compounds to sense Cr (III) by fluorescence spectroscopy.

4.2.3 Cr (III) Interference test

To determine if the sensing of Cr (III) had any interferents, mixtures containing Cr(III) and different metal ions were added to solutions of both compounds and compared to the addition of only Cr (III) to both compounds. As can be seen in **Figure 20a**, when the mixture of Cr (III) and different metal ions come in contact with **BTZ-COOH**, all the samples present complete quenching of the fluorescence. Cr (III) being a hard acid has a greater affinity to bind to the carboxylate, which is a hard base, hence the quenching of fluorescence in all the samples. The small fluorescence signal of the Cd (II) sample may be negligible,

thus **BTZ-COOH** does not have interferents. On the other hand, interference tests with **BTZ-O** revealed that Cu (II) increased the fluorescence of the sample while the change in intensity of other metals can be negligible. Cu (II) on its own did not have an effect in the photophysical properties of **BTZ-O**, thus the possible formation of a heterobimetallic complex can explain the increase in fluorescence, as these types of coordination compounds have presented unusual fluorescence properties like enhancement (62) or quenching (63) upon addition of a second metal ion.

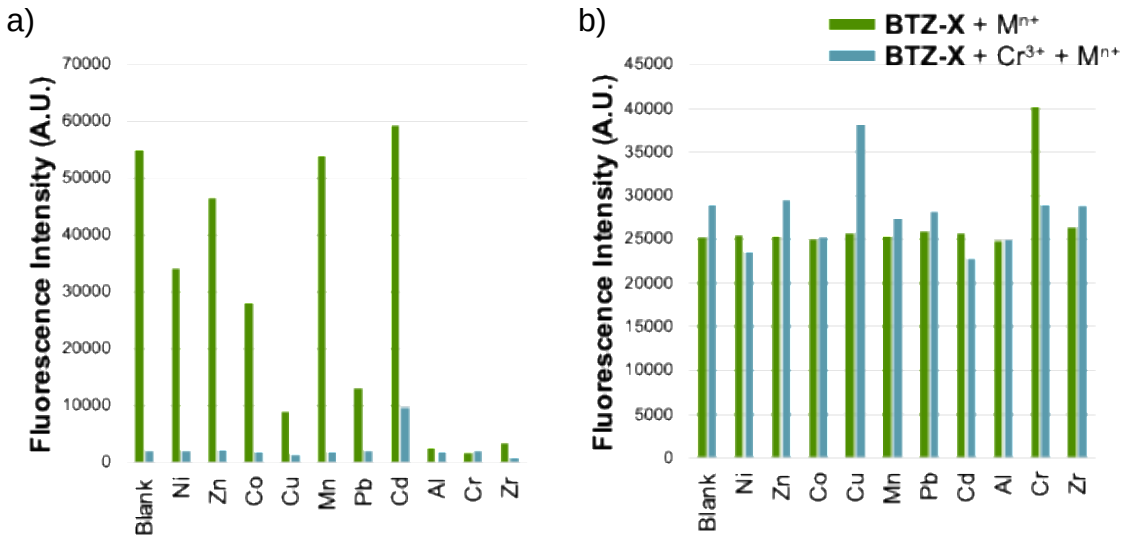

Figure 20. Fluorescence intensity of 4 mL of a) **BTZ-COOH** at 583 nm and b) **BTZ-O** at 505 nm (10 mM) in the presence of 5 eq of Cr (III) and 5 eq of different metal ions (100 mL of H_2O). λ_{ex}=353 nm for **BTZ-COOH**. λ_{ex}=413 nm for **BTZ-O**

4.2.4 Job's Plot

To determine the stoichiometry of Cr (III) sensing, mixtures with a total concentration of 10 μM and increasing molar fractions of Cr (III) were analyzed by fluorescence spectroscopy. The fluorescence intensity was plotted against the molar fraction of Cr (III) to build Job's Plot. As can be observed in **Figure 21**, the maximum fluorescence intensity for **BTZ-COOH** located at 0.4 molar fraction of Cr (III) can be attributed to a 2:3 (Cr:**BTZ-COOH**) stoichiometric relation. Meanwhile, the maximum fluorescence intensity for **BTZ-O** was located at 0.5

molar fraction of Cr (III), which can be attributed to a 1:1 (Cr:**BTZ-O**) stoichiometric relation. These results might suggest that for **BTZ-COOH**, the coordination happens between two metal centers and three different carboxylate syn-syn bridges (64). On the other hand, **BTZ-O** could bind to Cr (III) from the nitrogen at the second position of benzotriazole and a nitrogen from oxadiazole, forming a six-member cycle coordination compound. This type of coordination, denominated as chelation, where a polydentate ligand coordinates to a single metal ion, produces more stable coordination compounds than monodentate ligand (65).

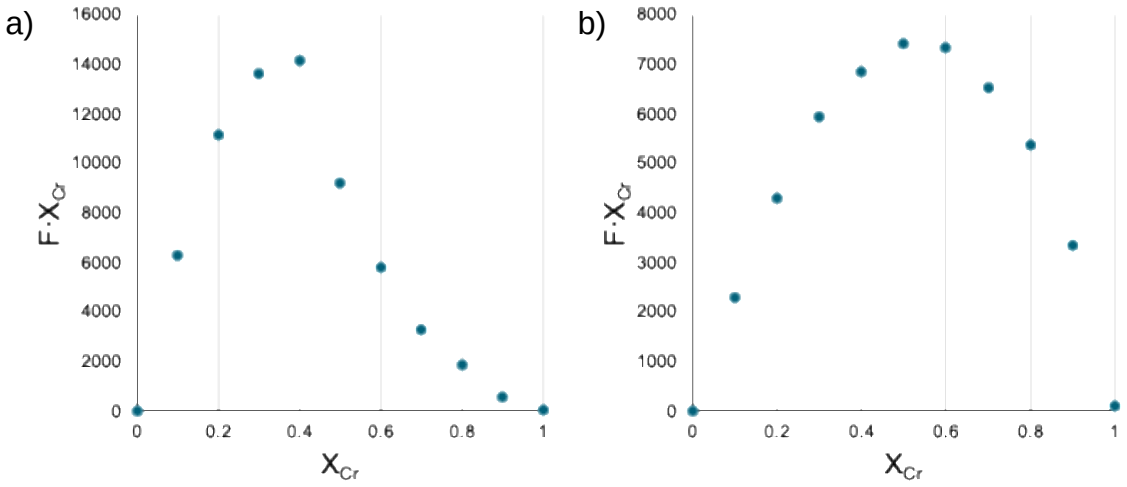

Figure 21. Job's plot for the sensor **BTZ-COOH** (a) and **BTZ-O** (b) with a total concentration of 10 μM. Fluorescence intensity at 583 nm for **BTZ-COOH** and 504 nm for **BTZ-O** was plotted as a function of the molar ratio of Cr (III). λ_{ex}=353 nm for **BTZ-COOH**, λ_{ex}=413 nm for **BTZ-O**.

4.2.5 Linear range and LOD

To further explore the sensing applicability of compounds **BTZ-X**, samples with varying concentrations of Cr (III) were prepared and analyzed by fluorescence spectroscopy in order to determine a linear range and LOD. As can be observed in **Figure 22**, the concentration of Cr (III) does not have a linear correlation to the fluorescence intensity, hence, the LOD could not be determined with this model. Likewise, other models like Benesi-Hildebrand and Stern-Volmer did not show a linear correlation between the data.

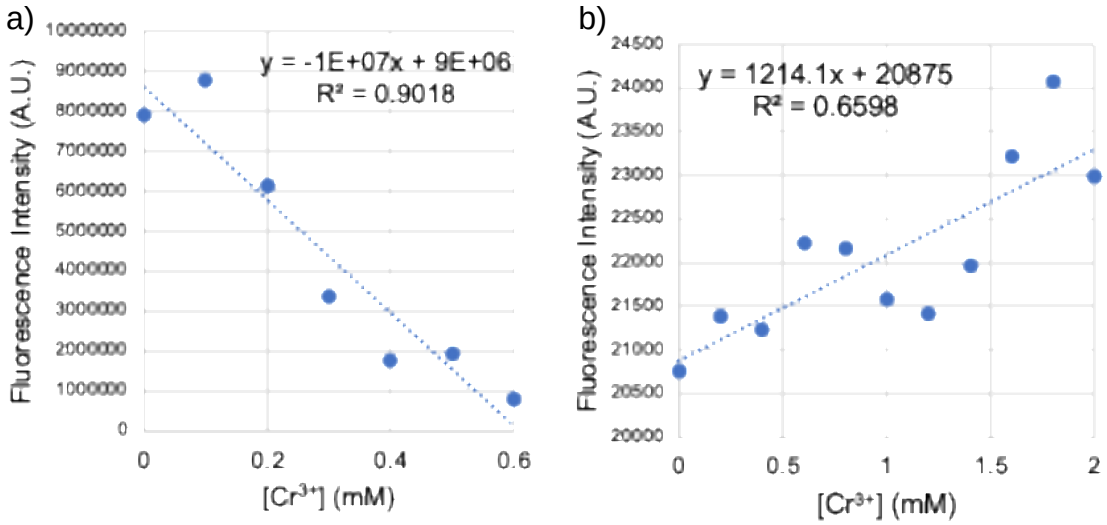

Figure 22. Calibration curve of 4 mL of a) **BTZ-COOH** and b) **BTZ-O** (10 mM) in the presence various concentrations of Cr (III) (100 μL of H_2O). λ_{ex}=353 nm for **BTZ-COOH**. λ_{ex} =413 nm for **BTZ-O**.

Even though the sensors did not show quantitative sensing capability for Cr (III), these compounds could still be used as qualitative sensors in solution or as a test strips. These methods could be used in the industrial sector as a mean to determine the presence of Cr (III) in wastewater before disposal (66) or determine if there are free Cr (III) ions inside cells that could lead to poisoning (67).

On the other hand, the synthetic protocols used for **BTZ-COOH** and **BTZ-O** could be adapted for the synthesis of molecules bearing benzotriazole or oxadiazole for other relevant applications. Based on the physicochemical and optoelectronic properties, these new compounds could be used as the emissive layer in OLEDs (high quantum yield and high thermal stability) (68), as a sensitizer in DSSC (high ε, λ_{max} > 400 nm and photostability) (69), as dye for cell imaging (ε > 30000 $M^{-1}cm^{-1}$ and SS> 80 nm) (70) or as a pharmaceutical (logP < 5 and negative binding energy between protein and compound) (71).

5 Conclusions

- The synthesis of **BTZ-COOH**, **BTZ-O**, and all their corresponding precursors was successful. The structures of all compounds were confirmed by NMR, HRMS and FT-IR.
- The photophysical properties of both compounds were determined. **BTZ-COOH** presented strong absorption at 379 nm and fluorescence at 583 nm. Meanwhile, **BTZ-O** presented strong absorption at 404 nm and fluorescence at 505 nm.
- **BTZ-COOH** showed bathochromic shifts in absorption wavelength with metals like Al (III), Cr (III) and Zr (IV); partial quenching of fluorescence with Al (III) and Zr (IV); and total quenching of fluorescence with Cr (III).
- **BTZ-O** showed no changes in absorption wavelength or intensity with other metals and enhancement of fluorescence was observed upon addition of Cr (III) ions.
- **BTZ-COOH** has no interferents for Cr (III) sensing. Meanwhile, Cu (II) is an interferent for Cr(III) sensing using **BTZ-O**.
- Stoichiometry for the coordination compounds was successfully determined by Job's Plot, showing a 2:3 (Cr:**BTZ-COOH**) ratio and a 1:1 (Cr:**BTZ-O**) ratio.
- The range evaluated for both compounds did not show a linear correlation, thus the LOD cannot be determined.
- The hypothesis is rejected because both compounds did not show a linear correlation and LOD could not be determined.

5.1 Recommendations

- Evaluate the compounds in solution or as test strips for the qualitative analysis of Cr (III).
- With further studies (cyclic voltammetry and thermogravimetric analysis) and based on the combination of optical and physicochemical properties, the compounds could be used in DSSC or OLEDs.

6 References

1. Uglietti C, Gabrielli P, Cooke CA, Vallelonga P, Thompson LG. Widespread pollution of the south american atmosphere predates the industrial revolution by 240 y. Proc Natl Acad Sci USA. 2015 Feb 24;112(8):2349–54.

2. Fuller R, Landrigan PJ, Balakrishnan K, Bathan G, Bose-O'Reilly S, Brauer M, et al. Pollution and health: a progress update. Lancet Planet Health. 2022 Jun 1;6(6):e535–47.

3. Diario Oficial de la Federación. Programa Nacional Hídrico 2020–2024.

4. Rahman Z, Singh VP. The relative impact of toxic heavy metals (THMs) (arsenic (As), cadmium (Cd), chromium (Cr)(VI), mercury (Hg), and lead (Pb)) on the total environment: an overview. Vol. 191, Environmental Monitoring and Assessment. Springer International Publishing; 2019.

5. IARC Working Group on the Evaluation of Carcinogenic Risks to Humans., International Agency for Research on Cancer. Chromium, nickel and welding. Vol. 49. Lyon: IARC; 1990. 49–214 p.

6. Barnhart J. Occurrences, Uses, and Properties of Chromium. Vol. 26, REGULATORY TOXICOLOGY AND PHARMACOLOGY. 1997.

7. Hossini H, Shafie B, Niri AD, Nazari M, Esfahlan AJ, Ahmadpour M, et al. A comprehensive review on human health effects of chromium: insights on induced toxicity. Vol. 29, Environmental Science and Pollution Research. Springer Science and Business Media Deutschland GmbH; 2022. p. 70686–705.

8. Agency for Toxic Substances and Disease Registry (ATSDR). Toxicological Profile for Chromium. Atlanta, GA; 2012.

9. Jaishankar M, Tseten T, Anbalagan N, Mathew BB, Beeregowda KN. Toxicity, mechanism and health effects of some heavy metals. Interdiscip Toxicol. 2014 Jun 1;7(2):60–72.

10. Liang J, Huang X, Yan J, Li Y, Zhao Z, Liu Y, et al. A review of the formation of Cr(VI) via Cr(III) oxidation in soils and groundwater. Vol. 774, Science of the Total Environment. Elsevier B.V.; 2021.

11. Tchounwou PB, Yedjou CG, Patlolla AK, Sutton DJ. Heavy metal toxicity and the environment. Vol. 101, EXS. 2012. p. 133–64.

12. National Research Counsil. Chromium. Washington, D.C.: National Academies Press; 1974.

13. Xu S, Yu C, Wang Q, Liao J, Liu C, Huang L, et al. Chromium Contamination and Health Risk Assessment of Soil and Agricultural Products in a Rural Area in Southern China. Toxics. 2023 Jan 1;11(1).

14. Wang L, Guo J, Zhang W, Chen B, Wang H, Li H. Pollution Levels for Airborne Hexavalent Chromium of PM2.5 in Typical Cities of China. Atmosphere (Basel). 2023 Feb 1;14(2).

15. Chhikara A, Tomar D, Bartwal G, Chaurasia M, Husain Z, College D. Thiadiazole Functionalized Salicylaldehyde-Schiff Base as a pH-responsive and Chemo-Reversible “Turn-Off” Fluorescent probe for Selective Cu (II) Detection: Logic Gate Behaviour and Molecular Docking Studies. J Fluoresc. 2022;1–26.

16. Szekeres L. Determination of Chromium by EDTA Titration. MICROCHEMICAL JOURNAL. 1972;17:360–3.

17. Hartley FR. The Titrimetric Determination of Chromium in the Presence of Excess of Chloride. Vol. 94, Analyst. 1969.

18. Erdey L. Gravimetric Analysis Part II. 1st ed. Buzás I, editor. Pergamon Press; 1965.

19. Sanchez-Hachair A, Hofmann A. Hexavalent chromium quantification in solution: Comparing direct UV–visible spectrometry with 1,5-diphenylcarbazide colorimetry. Comptes Rendus Chimie. 2018 Sep 1;21(9):890–6.

20. Shirani M, Salari F, Habibollahi S, Akbari A. Needle hub in-syringe solid phase extraction based a novel functionalized biopolyamide for simultaneous green separation/preconcentration and determination of cobalt, nickel, and chromium (III) in food and environmental samples with micro sampling flame atomic absorption spectrometry. Microchemical Journal. 2020 Jan 1;152:104340.

21. Frois SR, Tadeu Grassi M, De Campos MS, Abate G. Determination of Cr(VI) in water samples by ICP-OES after separation of Cr(III) by montmorillonite. Analytical Methods. 2012 Dec;4(12):4389–94.

22. Skoog DA, Holler FJ, Crouch SR. Principios de analisis intrumental. 6th ed. Vol. 1. 2008.

23. Che W, Xie Y, Li Z. Structural Design of Blue-to-Red Thermally-Activated Delayed Fluorescence Molecules by Adjusting the Strength between Donor and Acceptor. Vol. 9, Asian Journal of Organic Chemistry. Wiley-VCH Verlag; 2020. p. 1262–76.

24. Abdurahman A, Obolda A, Peng Q, Li F. Efficient deep blue fluorescent OLEDs with ultra-low efficiency roll-off based on 4H-1,2,4-triazole cored D-A and D-A-D type emitters. Dyes and Pigments. 2018 Jun 1;153:10–7.

25. Pu YR, Chen Y. Solution-processable bipolar hosts based on triphenylamine and oxadiazole derivatives: Synthesis and application in phosphorescent light-emitting diodes. J Lumin. 2016;170(1):127–35.

26. Zhang XH, Liu Q, Shi HJ, Wang LY, Fu YL, Wei XC, et al. Synthesis, spectral properties of cell-permeant dimethine cyanine dyes and their application as fluorescent probes in living cell imaging and flow cytometry. Dyes and Pigments. 2014;100(1):232–40.

27. Liu Z, Liu D, Zhang K, Zhu T, Zhong Y, Li F, et al. Efficient fullerene-free solar cells with wide optical band gap polymers based on fluorinated benzotriazole and asymmetric benzodithiophene. J Mater Chem A Mater. 2017;5:21650–7.

28. Li Q, Wang Z, Song W, Ma H, Dong J, Quan YY, et al. A novel D-π-A triphenylamine-based turn-on colorimetric and ratiometric fluorescence probe for cyanide detection. Dyes and Pigments. 2019 Feb 1;161:389–95.

29. Li Y, Hou J, Zhou H, Jia M, Chen S, Huang H, et al. A fluorescence sensor array based on perylene probe monomer-excimer emission transition for the highly efficient differential sensing of metal ions and drinking waters. Sens Actuators B Chem. 2020 Sep 15;319(1):1–12.

30. Liu Z, He W, Guo Z. Metal coordination in photoluminescent sensing. Chem Soc Rev. 2013 Jan 28;42(4):1568–600.

31. Lee H, Hancock RD, Lee HS. Role of fluorophore-metal interaction in photoinduced electron transfer (PET) sensors: Time-dependent density functional theory (TDDFT) study. Journal of Physical Chemistry A. 2013 Dec 19;117(50):13345–55.

32. Borase PN, Thale PB, Shankarling GS. Dihydroquinazolinone based “turn-off” fluorescence sensor for detection of Cu^{2+} ions. Dyes and Pigments. 2016 Nov 1;134:276–84.

33. Karak D, Banerjee A, Sahana A, Guha S, Lohar S, Adhikari SS, et al. 9-Acridone-4-carboxylic acid as an efficient Cr(III) fluorescent sensor: Trace level detection, estimation and speciation studies. J Hazard Mater. 2011 Apr 15;188(1–3):274–80.

34. Seenan S, Manickam S, Kulathu Iyer S. A new furan based fluorescent chemosensor for the recognition of Cr^{3+} ion and its application in real sample analysis. J Photochem Photobiol A Chem. 2021 Sep 1;418.

35. Kolcu F, Erdener D, Kaya İ. A Schiff base based on triphenylamine and thiophene moieties as a fluorescent sensor for Cr (III) ions: Synthesis, characterization and fluorescent applications. Inorganica Chim Acta. 2020 Sep 1;509.

36. Singh G, Singh R, George N, Singh G, Sushma, Kaur G, et al. 'Click'-synthesized PET based fluorescent sensor for Hg(II), Pb(II) and Cr(III) recognition: DFT and docking studies. J Photochem Photobiol A Chem. 2023 Jul 1;441.

37. Liu Y, Yang F, Wei K, Kang M, Liu P, Yang X, et al. 5-(Thiophene-2-yl)oxazole derived "off-on-off" fluorescence chemosensor for sequential recognition of In^{3+} and Cr^{3+} ions. J Photochem Photobiol A Chem. 2023 Mar 1;437.

38. Homocianu M, Airinei A, Ipate AM, Hamciuc C. Spectroscopic Recognition of Metal Ions and Non-Linear Optical (NLO) Properties of Some Fluorinated Poly(1,3,4-Oxadiazole-Ether)s. Chemosensors. 2022 May 1;10(5):1–16.

39. Su K, Huang X, Wei W, Zeng X, Xiang S, Yang H. A ready-to-use fluorescence probe of Pd^{2+} in water: novel tricyclic heterocyclic base on 1,3,4-oxadiazole. Luminescence. 2021 Nov 1;36(7):1690–6.

40. Gong X, Zhang H, Jiang N, Wang L, Wang G. Oxadiazole-based 'on-off' fluorescence chemosensor for rapid recognition and detection of Fe^{2+} and Fe^{3+} in aqueous solution and in living cells. Microchemical Journal. 2019 Mar 1;145:435–43.

41. Naik L, Maridevarmath C V., Thippeswamy MS, Savanur HM, Khazi IAM, Malimath GH. A highly selective and sensitive thiophene substituted 1,3,4-oxadiazole based turn-off fluorescence chemosensor for Fe2+and turn on fluorescence chemosensor for Ni^{2+} and Cu^{2+} detection. Mater Chem Phys. 2021 Feb 15;260.

42. Najare MS, Patil MK, Garbhagudi M, Yaseen M, Inamdar SR, Khazi IAM. Design, synthesis and characterization of π-conjugated 2,5-diphenylsubstituted-1,3,4-oxadiazole-based D-π-A-π'-D′ form of efficient deep blue functional materials: Photophysical properties and fluorescence "Turn-off" chemsensors approach. J Mol Liq. 2021 Apr 15;328.

43. Dolai B, Nayim S, Hossain M, Pahari P, Kumar Atta A. A triazole linked C-glycosyl pyrene fluorescent sensor for selective detection of Au^{3+} in

aqueous solution and its application in bioimaging. Sens Actuators B Chem. 2019 Jan 15;279:476–82.

44. Singh G, Satija P, Singh A, Diksha, Pawan, Suman, et al. Azo dye featuring triazole appended organosilicon multifunctionalized sensor: Paradigm for detection of Cu^{+2} and Fe^{+2} ions. Mater Chem Phys. 2020 Jul 15;249.

45. Singh G, Priyanka, Sushma, Pawan, Mohit, Satija P, et al. Synthesis and Characterization of Antioxidant Biphenyl Appended 1,2,3-Triazoles as Potential Chemo-Sensor for Sn^{2+} Ions: Excellent Selectivity and Low Detection Limit. ChemistrySelect. 2021 Aug 13;6(30):7613–21.

46. Zhao H, Kang H, Fan C, Liu G, Pu S. A new multi-functional fluorescent mercuric ion sensor based on diarylethene with triazole-linked rhodamine B unit. Tetrahedron. 2020 Aug 14;76(33).

47. Rout K, Manna AK, Sahu M, Mondal J, Singh SK, Patra GK. Triazole-based novel bis Schiff base colorimetric and fluorescent turn-on dual chemosensor for Cu^{2+} and Pb^{2+}: Application to living cell imaging and molecular logic gates. RSC Adv. 2019;9(44):25919–31.

48. Liu J, Meng X, Duan H, Xu T, Ding Z, Liu Y, et al. Two Schiff-base fluorescence probes based on triazole and benzotriazole for selective detection of Zn^{2+}. Sens Actuators B Chem. 2016 May 1;227:296–303.

49. Wang Y, Liu S, Chen H, Liu Y, Li H. A novel “turn-on” fluorescence probe based on azoaniline-arylimidazole dyad for the detection of Cu^{2+}. Dyes and Pigments. 2017 Jul 1;142:293–9.

50. Gupta M, Lee PH il. A dual responsive molecular probe for the efficient and selective detection of nerve agent mimics and copper (II) ions with controllable detection time. Sens Actuators B Chem. 2017;242:977–82.

51. Senthamarai T, Chandrashekhar VG, Rockstroh N, Rabeah J, Bartling S, Jagadeesh R V., et al. A “universal” catalyst for aerobic oxidations to synthesize (hetero)aromatic aldehydes, ketones, esters, acids, nitriles, and amides. Chem. 2022 Feb 10;8(2):508–31.

52. Noushini S, Park SJ, Perez J, Holgate D, Mendez V, Jamie IM, et al. Electrophysiological responses of bactrocera kraussi (Hardy) (tephritidae) to rectal gland secretions and headspace volatiles emitted by conspecific males and females. Molecules. 2021 Aug 2;26(16).

53. Ran CK, Liao LL, Gao TY, Gui YY, Yu DG. Recent progress and challenges in carboxylation with CO2. Vol. 32, Current Opinion in Green and Sustainable Chemistry. Elsevier B.V.; 2021.

54. El Mansouri A eddine, Oubella A, Dânoun K, Ahmad M, Neyts J, Jochmans D, et al. Discovery of novel furo[2,3-d]pyrimidin-2-one–1,3,4-oxadiazole hybrid derivatives as dual antiviral and anticancer agents that induce apoptosis. Arch Pharm (Weinheim). 2021 Oct 1;354(10).

55. Kaur K, Verma H, Gangwar P, Jangid K, Dhiman M, Kumar V, et al. Design, synthesis, in silico and biological evaluation of new indole based oxadiazole derivatives targeting estrogen receptor alpha. Bioorg Chem. 2024 Jun 1;147.

56. Donnelly K, Baumann M. Flow synthesis of oxadiazoles coupled with sequential in-line extraction and chromatography. Beilstein Journal of Organic Chemistry. 2022;18:232–9.

57. Doddagaddavalli MA, Kalalbandi VKA, Seetharamappa J, Joshi SD. New thiophene-1,3,4-oxadiazole-thiazolidine-2,4-dione hybrids: Synthesis, MCF-7 inhibition and binding studies. Bioorg Chem. 2024 Feb 1;143.

58. Ortega-Villarreal AS, Hernández-Fernández E, Jensen C, Valdivia-Berroeta GA, Garrard S, López I, et al. Synthesis and characterization of ethyl benzotriazolyl acrylate-based D-π-A fluorophores for live cell-based imaging applications. RSC Adv. 2019;9(16):8759–67.

59. Hernández-Fernández E, Ortega-Villarreal AS, García-López MC, Chan-Navarro R, Garrard S, Valdivia-Berroeta GA, et al. Synthesis and characterization of benzotriazolyl acrylonitrile analogs-based donor-acceptor molecules: Optical properties, in vitro cytotoxicity, and cellular imaging. Dyes and Pigments. 2021;189(May 2021):1–10.

60. Yang J, Duan J, Wang G, Zhou H, Ma B, Wu C, et al. Visible-Light-Promoted Site-Selective N1-Alkylation of Benzotriazoles with α-Diazoacetates. Org Lett. 2020 Sep 18;22(18):7284–9.

61. Karimian A, Emarloo N, Salari S. The mineral alum: an effective and low-cost heterogeneous catalyst for the successful synthesis of 5-substituted-1H-tetrazoles. Inorganic and Nano-Metal Chemistry. 2021 Jan 2;51(1):91–100.

62. Liu C, An XX, Cui YF, Xie KF, Dong WK. Novel structurally characterized hetero-bimetallic [Zn(II)2M(II)] (M = Ca and Sr) bis(salamo)-type complexes: DFT calculation, Hirshfeld analyses, antimicrobial and fluorescent properties. Appl Organomet Chem. 2020 Jan 1;34(1).

63. Zhang T, Li W Da, Li X, Peng YD, Dong WK. Unusual fluorescence behavior of first 3d-3d′ heterobimetallic [Cu(II)$_2$Mn(II)] complex bearing a bis(salamo)-based ligand. J Mol Struct. 2022 Jul 15;1260.

64. Mikuriya M, Yamakawa C, Tanabe K, Nukita R, Amabe Y, Yoshioka D, et al. Copper(Ii) carboxylates with 2,3,4-trimethoxybenzoate and 2,4,6-trimethoxybenzoate: Dinuclear Cu(II) cluster and μ-aqua-bridged Cu(II) chain molecule. Magnetochemistry. 2021 Mar 1;7(3).

65. Gulcin İ, Alwasel SH. Metal Ions, Metal Chelators and Metal Chelating Assay as Antioxidant Method. Vol. 10, Processes. MDPI; 2022.

66. Iftikhar R, Parveen I, Ayesha, Mazhar A, Iqbal MS, Kamal GM, et al. Small organic molecules as fluorescent sensors for the detection of highly toxic heavy metal cations in portable water. J Environ Chem Eng. 2023 Feb 1;11(1).

67. Goshisht MK, Patra GK, Tripathi N. Fluorescent Schiff base sensors as a versatile tool for metal ion detection: strategies, mechanistic insights, and applications. Vol. 3, Materials Advances. Royal Society of Chemistry; 2022. p. 2612–69.

68. Pfeifer G, Chahdoura F, Papke M, Weber M, Szűcs R, Geffroy B, et al. Synthesis, Electronic Properties and OLED Devices of Chromophores Based on λ_5-Phosphinines. Chemistry - A European Journal. 2020 Aug 17;26(46):10534–43.

69. Rahman S, Haleem A, Siddiq M, Hussain MK, Qamar S, Hameed S, et al. Research on dye sensitized solar cells: recent advancement toward the various constituents of dye sensitized solar cells for efficiency enhancement and future prospects. Vol. 13, RSC Advances. Royal Society of Chemistry; 2023. p. 19508–29.

70. Yang L, Chen S, Yi D, Chen Q, Zhang J, Xie Y, et al. Synthesis and fluorescence properties of red-to-near-infrared-emitting push-pull dyes based on benzodioxazole scaffolds. J Mater Chem B. 2021 Oct 28;9(40):8512–7.

71. Abdellah IM, Eletmany MR, Abdelhamid AA, Alghamdi HS, Abdalla AN, Elhenawy AA, et al. One-pot synthesis of novel poly-substituted 3-cyanopyridines: Molecular docking, antimicrobial, cytotoxicity, and DFT/TD-DFT studies. J Mol Struct. 2023 Oct 5;1289.

7 Supplementary Information

Ethyl 2-(2*H*-benzotriazol-2-yl)acetate **2a**. (12%)

White solid, mp 122–124 ºC; ^{1}H-NMR (500 MHz, $CDCl_3$): δ 1.27 (t, J= 7.1 Hz, 3H), 4.27 (q, J= 7.1 Hz, 2H), 5.53 (s, 2H, CH_2COOEt), 7.38-7.42 (m, 2H, H_{arom}), 7.86-7.90 (m, 2H, H_{arom}); ^{13}C-NMR (125 MHz, $CDCl_3$): δ 14.1, 57.2, 62.5, 118.3, 127.0, 145.0, 166.3. HRMS (ESI^+) *m/z* calcd for $C_{10}H_{12}N_3O_2$ $[M + H]^+$ 206.09295, found 206.09214.

Ethyl 2-(1*H*-benzotriazol-2-yl)acetate **2**. (88%)

White solid, mp 83-84 ºC; ^{1}H-NMR (500 MHz, $CDCl_3$): δ 1.26 (t, J= 7.1 Hz, 3H), 4.25 (q, J= 7.1 Hz, 2H), 5.42 (s, 2H, CH_2COOEt), 7.38-7.53 (m, 3H, H_{arom}), 8.08 (d, J= 8.4 Hz, 1H, H_{arom}); ^{13}C-NMR (125 MHz, $CDCl_3$): δ 14.1, 49.1, 62.3, 109.2, 120.2, 124.1, 127.9, 133.4, 146.0, 166.4. HRMS (ESI^+) *m/z* calcd for $C_{10}H_{12}N_3O_2$ $[M + H]^+$ 206.09295, found 206.09223.

Ethyl (*Z*)-2-(1*H*-benzotriazol-1-yl)-3-(4-(dimethylamino)phenyl)acrylate **3**. (35%)

Yellow solid, mp 152–154 ºC; ^{1}H-NMR (300 MHz, $CDCl_3$): δ 1.19 (t, J= 7.1 Hz, 3H), 2.91 (s, 6H, $(CH_3)_2N$), 4.23 (q, J= 7.1 Hz, 2H), 6.36 (d, J= 9.1Hz, 2H, H_{arom}), 6.58 (d, J= 9.1Hz, 2H, H_{arom}), 7.29–7.48 (m, 3H, H_{arom}), 8.11 (s, 1H, $H_{vinylic}$), 8.15 (d, J= 7.4 Hz, 1H H_{arom}); ^{13}C-NMR (125 MHz, $CDCl_3$): δ 14.2, 39.8, 61.5, 110.1, 111.5, 117.7, 118.2, 119.9, 124.1, 128.0, 132.8, 133.6, 142.2, 145.8, 152.1, 164.3. HRMS (ESI^+) *m/z* calcd for $C_{19}H_{21}N_4O_2$ $[M + H]^+$ 337.16645, found 337.16540.

(*Z*)-2-(1*H*-benzotriazol-1-yl)-3-(4-(dimethylamino)phenyl)acrylic acid **BTZ-COOH.** (74%)

^{1}H-NMR (500 MHz, $CDCl_3/CD_3OD$): δ 2.84 (s, 6H, $(CH_3)_2N$), 6.29 (d, *J*=8.6 Hz, 2H,H_{arom}), 6.46 (d, *J*=8.6 Hz, 2H, H_{arom}), 7.29 (d, *J*=8.2 Hz, 1H, H_{arom}), 7.32-7.40 (m,2H, H_{arom}), 8.03 (d, *J* = 8.3 Hz, 1H, H_{arom}); 8.07 (s, 1H, $H_{vinylic}$); ^{13}C-NMR (125 MHz, $CDCl_3/CD_3OD$): δ 39.6, 110.3, 111.4, 117.3, 118.0, 119.4, 124.4, 128.2, 132.7,133.5, 142.7, 145.3, 152.2, 166.1. HRMS (ESI^+) *m/z* calcd for $C_{17}H_{17}N_4O_2$ $[M+H]^+$ 309.13515, found 309.13272.

2-(2*H*-benzotriazol-2-yl)acetonitrile **4a**. (25%)

Beige solid, mp 78–80 ◦C; ^{1}H-NMR (500 MHz, CD_3OD): δ 4.86 (s, 2H, CH_2CN), 7.40–7.48 (m, 2H, H_{arom}), 7.82–7.89 (m, 2H, H_{arom}); ^{13}C-NMR (125 MHz, $CDCl_3$): δ 43.9, 114.5, 119.0, 128.5, 146.2. HRMS (ESI^+) *m/z* calcd for $C_8H_6N_4$ $[M+H]^+$ 159.06707, found 159.06716.

2-(1*H*-benzotriazol-1-yl)acetonitrile **4**. (75%)

Beige solid, mp 86–87 ◦C; ^{1}H-NMR (700 MHz, CD_3OD): δ 5.96 (s, 2H, CH_2CN), 7.46 (t, 1H, H_{arom}), 7.61 (t, 1H, H_{arom}), 7.82 (d, J =8.4 Hz, 1H, H_{arom}), 8.01 (d, J =8.4 Hz, 1H, H_{arom}); ^{13}C NMR (175 MHz, CD_3OD): δ 36.4, 110.7, 114.9, 120.5, 126.1, 129.8, 133.9, 146.8. HRMS (ESI^+) *m/z* calcd for $C_8H_6N_4$ $[M+H]^+$ 159.06707, found 159.06712.

(*E*)-2-(1*H*-benzotriazol-2-yl)-3(4(dimethylamino)phenyl)acrylonitrile **5**. (79%)

Yellow-orange solid, mp 186–188 ◦C, ^{1}H-NMR (700 MHz, $CDCl_3$): δ 3.10 (s, 6H, $(CH_3)_2N$), 6.75 (d, J =9.0 Hz, 2H, H_{arom}), 7.42–7.48 (m, 1H, H_{arom}), 7.56–7.62 (m, 1H, H_{arom}), 7.66 (s, 1H, $H_{vinylic}$), 7.82-7.88 (m, 3H, H_{arom}), 8.12 (d, J =8.4 Hz, 1H, H_{arom}); ^{13}C-NMR (175 MHz, $CDCl_3$): δ 40.1, 99.5, 110.4, 111.8, 115.6, 117.7, 120.5, 124.8, 128.7, 132.1, 132.3, 143.0, 146.2, 152.8. HRMS (ESI^+) *m/z* calcd for $C_{17}H_{15}N_5$ $[M+H]^+$ 290.14057, found 290.14083.

(*E*)-4-(2-(1*H*-benzotriazol-1-yl)-2-(1*H*-tetrazol-5-yl)vinyl)-*N*,*N*-dimethylaniline **6**. (35%)

Orange solid, mp>260 ºC, ^{1}H-NMR (700 MHz, DMSO-d6): δ 2.86 (s, 6H, $(CH_3)_2N$), 3.42 (bs, 1H, NH), 6.43-6.55 (m, 4H, H_{arom}), 7.43 (d, *J*=8.1 Hz, 1H, H_{arom}), 7.48–7.58 (m, 2H, H_{arom}), 8.08 (s, 1H, $H_{vinylic}$), 8.26 (d, *J* =8.1 Hz, 1H, H_{arom}). HRMS (ESI^+) *m/z* calcd for $C_{17}H_{16}N_8$ $[M+H]^+$ 333.1571, found 333.1555.

(*E*)-4-(2-(1*H*-benzotriazol-1-yl)-2-(5-phenyl-1,3,4-oxadiazol-2-yl)vinyl)-N,N-dimethylaniline **BTZ-O.** (53%)

Yellow solid, mp>260 ºC, ^{1}H-NMR (700 MHz, $CDCl_3$): δ 2.92 (s, 6H, $(CH_3)_2N$), 6.39 (d, *J*=8.4 Hz, 2H, H_{arom}), 6.63 (d, *J*=8.3 Hz, 2H, H_{arom}), 7.36 (d, *J*=7.9 Hz, 1H, H_{arom}), 7.42–7.53 (m, 5H, H_{arom}), 7.97 (d, *J*=6.9 Hz, 2H, H_{arom}), 8.00 (s, 1H, $H_{vinylic}$), 8.21 (d, J = 8.0 Hz, 1H, H_{arom}); ^{13}C-NMR (175 MHz, $CDCl_3$) δ 39.83, 110.18, 111.67, 112.33, 118.64, 120.29, 123.65, 124.42, 126.95, 128.49, 129.00, 131.72, 132.28, 133.29, 136.97, 145.94, 151.89, 163.11, 164.33. HRMS (ESI^+) *m/z* calcd for $C_{24}H_{20}N_6O$ $[M+H]^+$ 409.1771, found 409.1777.

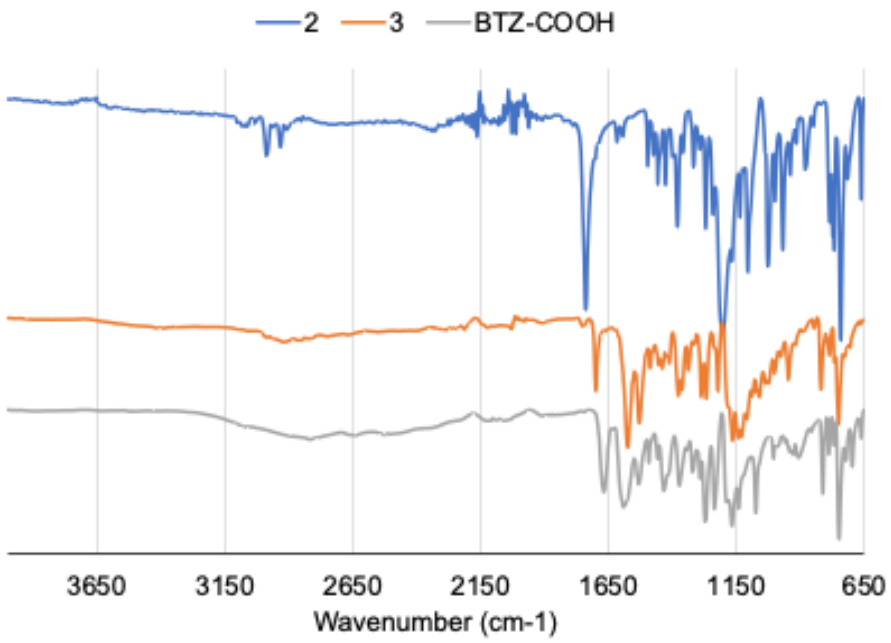

SI 1. Comparison of FT-IR spectra of precursors to **BTZ-COOH**.

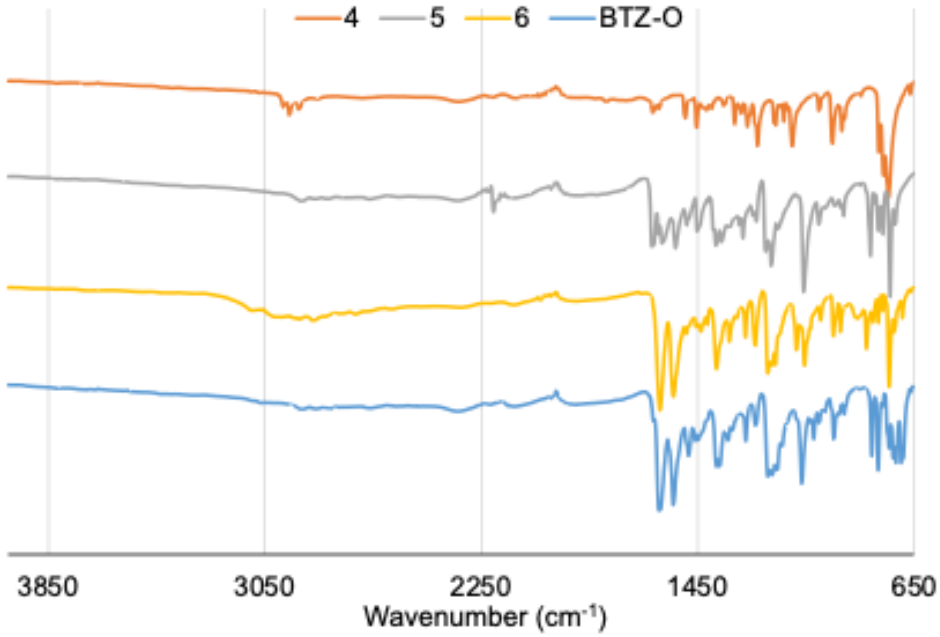

SI 2. Comparison of FT-IR spectra of precursors to **BTZ-O**.